(2)

AFWAL-TR-83-4140

ML12 Spacecraft Contamination and Coatings Degradation Flight Experiment

David F. Hall

The Aerospace Corporation
El Segundo, CA 90245

December 1983

INTERIM REPORT FOR PERIOD
23 Dec 1974–30 Sept 1983

Approved for public release; distribution unlimited.

MATERIALS LABORATORY
AIR FORCE WRIGHT AERONAUTICAL LABORATORIES
AIR FORCE SYSTEMS COMMAND
WRIGHT-PATTERSON AIR FORCE BASE, OHIO 45433

NOTICE

When Government drawings, specifications, or other data are used for any purpose other than in connection with a definitely related Government procurement operation, the United States Government thereby incurs no responsibility nor any obligation whatsoever; and the fact that the Government may have formulated, furnished, or in any way supplied the said drawings, specifications, or other data, is not to be regarded by implication or otherwise as in any manner licensing the holder or any other person or corporation, or conveying any rights or permission to manufacture, use, or sell any patented invention that may in any way be related thereto.

This technical report has been reviewed and is approved for publication.

Ray A Cull
1Lt Ray A. Cull
Project Engineer

B. D. McConnell
B. D. McConnell, Chief
Nonstructural Materials Branch

For the Commander:

F. D. Cherry
F. D. Cherry, Chief
Nonmetallic Materials Division

If your address has changed, if you wish to be removed from our mailing list, or if the addressee is no longer employed by our organization please notify AFWAL/MLBT, Wright Patterson AFB, OH 45433 to help maintain a current mailing list.

Copies of this report should not be returned unless return is required by security considerations, contractual obligations, or notice on a specific document.

UNCLASSIFIED

SECURITY CLASSIFICATION OF THIS PAGE *(When Data Entered)*

REPORT DOCUMENTATION PAGE	READ INSTRUCTIONS BEFORE COMPLETING FORM
1. REPORT NUMBER AFWAL-TR-83-4140	2. GOVT ACCESSION NO. AD-A150095	3. RECIPIENT'S CATALOG NUMBER
4. TITLE *(and Subtitle)* ML12 SPACECRAFT CONTAMINATION AND COATINGS DEGRADATION FLIGHT EXPERIMENT.	5. TYPE OF REPORT & PERIOD COVERED Interim 6. PERFORMING ORG. REPORT NUMBER TR-0084(4510)-1
7. AUTHOR(s) David. F. Hall	8. CONTRACT OR GRANT NUMBER(s) F04701-83-C-0084
9. PERFORMING ORGANIZATION NAME AND ADDRESS The Aerospace Corporation El Segundo, Calif. 90245	10. PROGRAM ELEMENT, PROJECT, TASK AREA & WORK UNIT NUMBERS ILIR 0070
11. CONTROLLING OFFICE NAME AND ADDRESS Air Force Wright Aeronautical Laboratory Wright-Patterson Air Force Base, Ohio 45433	12. REPORT DATE December 1983 13. NUMBER OF PAGES 87
14. MONITORING AGENCY NAME & ADDRESS *(if different from Controlling Office)* Space Division Los Angeles Air Force Station Los Angeles, Calif. 90009	15. SECURITY CLASS. *(of this report)* Unclassified 15a. DECLASSIFICATION/DOWNGRADING SCHEDULE

16. DISTRIBUTION STATEMENT *(of this Report)*

Approved for public release; distribution unlimited.

17. DISTRIBUTION STATEMENT *(of the abstract entered in Block 20, if different from Report)*

18. SUPPLEMENTARY NOTES

19. KEY WORDS *(Continue on reverse side if necessary and identify by block number)*

Spacecraft Contamination	SCATHA
Thermal Control Coatings	Rocket Plume Contamination
Quartz Crystal Microbalance (QCM)	Optical Solar Reflector (OSR)
Calorimeter	Optical Effects of Contamination
Spacecraft Charging	

20. ABSTRACT *(Continue on reverse side if necessary and identify by block number)*

The ML12 experiment was launched ~~on January~~ 30, 1979, on the ~~United States Air Force (USAF)~~ Space Test Program P78-2 spacecraft, ~~which is~~ sometimes called SCATHA. It was designed to determine if spacecraft charging contributes significantly to the rate that contaminants arrive at exterior spacecraft surfaces, and to establish some of the characteristics and effects of these contaminants. Two sensor types are used in the experiment: (1) →

DD FORM 1473 (FACSIMILE)

UNCLASSIFIED

SECURITY CLASSIFICATION OF THIS PAGE *(When Data Entered)*

19. KEY WORDS (Continued)

20. ABSTRACT (Continued)

One type is a combination retarding potential analyzer (RPA) and temperature controlled quartz crystal microbalance (TQCM). With it, distinction can be made between charged and uncharged arriving molecules, and information can be obtained concerning the temperature dependence of contaminant adsorption and desorption rates. The other sensor type is a tray of calorimetrically mounted thermal control coating (TCC) samples. Samples of different spacecraft surface materials are exposed to arriving contaminants, and the solar absorptances (α_s) of these materials are continuously measured. The two RPA/TQCMs are both accumulating mass, but the accumulation rates and characteristics of the mass differ. Ultraviolet from the sun is the likely reason. Non-line-of-sight contamination transport has been found to be important at geosynchronous altitudes. With one exception, the early orbital values of α_s are in good agreement with prelaunch values indicating there was little contamination during prelaunch activities. The very small change in α_s for an OSR and other space-stable samples indicates that the SCATHA spacecraft was exceptionally clean. As a result, large α_s changes for other TCCs are attributed to the effects of radiation damage.

PREFACE

This work was largely supported by the Air Force Wright Aeronautical Laboratory (AFWAL/MLBE) under Space Division Contract F04701-83-C-0084 and preceding contracts. At AFWAL, this activity is known as ILIR 0070 (SCATHA). The Project Element is 62102F.

Undertakings as large as a flight experiment usually require the labors of many people; in this instance the numbers exceeded three dozen, all of whom made important contributions. The following individuals are due special thanks for their assistance: D. Prince, AFML, TCC sample procurement, measurement, and mounting and sponsor representative; W. Chater, Aerospace Corp., design and fabrication of much of the flight electronics; D. Jones, Aerospace Corp., mechanical fabrication, design and testing; P. Fleischauer, Aerospace Corp., assistance with program management and testing; R. Corbin, J. Goldman, J. Hribar, and W. Kalinowski, Aerospace Corp., calibration and environmental testing; D. Clark, Aerospace Corp., system testing and orbital operations; D. Boucher and A. A. Fote, Aerospace Corp., flight data software; J. Vellinga, Martin Marietta Aerospace, payload integration. The authors of Refs. 24 and 37 supplied important portions of the flight hardware under contract to AFML.

When the flight data became available, A. A. Fote, D. M. Clark, and D. J. Carré of The Aerospace Corporation made major contributions to the analysis and interpretation of various portions of the data. Assistance with data processing and analysis has been provided at various times by S. W. Ritter, M. Melton, J. N. Wakimoto, S. Goldberg, D. J. Mabry, A. E. Johnson, and J. Kordan, all of The Aerospace Corporation.

Finally, special recognition is due the MCC-F Mission Control Team of the Air Force Satellite Test Center for diligent and expert flight operations.

CONTENTS

I. INTRODUCTION..... 1

1. Program Goals..... 1
2. Spacecraft Description..... 3
3. Overview of ML12 Instruments..... 3
4. Spacecraft Cleanliness Requirements..... 6

II. THERMAL CONTROL COATINGS EXPERIMENT..... 10

1. Instrument Design..... 10
2. Sample Selection..... 13
3. Data Reduction..... 15
4. Preflight Calibrations and Calculations..... 17
5. Telemetry Quantization Errors..... 20
6. Flight Results..... 22
7. Summary..... 33

III. RETARDING POTENTIAL ANALYZER/ TEMPERATURE CONTROLLED QUARTZ CRYSTAL MICROBALANCE EXPERIMENT..... 35

1. Instrument Design..... 35
2. Data Reduction..... 41
3. Flight Results..... 44

IV. SUMMARY AND CONCLUSIONS..... 72

REFERENCES..... 79

LIST OF ILLUSTRATIONS

1. Negatively Charged Vehicle Reattracting Contaminant..... 2

2. P78-2 Space Vehicle..... 4

3. P78-2 Spacecraft with Locations of TCC Trays, Hydrazine Rocket Engine Modules, and Apogee Insertion Motor Cavity..... 8

4. Flight TCC Tray..... 11

5. Arrangement for Mounting TCC Sample Disks in Cup..... 12

6. Solar Absorptances of Black Paint Samples from Day of Launch..... 23

7. Solar Absorptances of Polished Aluminum Samples from Day of Launch..... 24

8. Solar Absorptances of Standard and In_2O_3-Coated Fused Silica Mirror Samples from Day of Launch..... 25

9. Solar Absorptances of 2- and 5-Mil Thick Silvered FEP-Teflon Samples from Day of Launch..... 26

10. Solar Absorptances of Plain, Gold-Coated, and In_2O_3-Coated Aluminized Kapton Samples from Day of Launch..... 27

11. Solar Absorptances of Astroquartz Fabric Samples Backed with Silvered Teflon and Double Adhesive Tape from Day of Launch..... 28

12. Solar Absorptances of Grafoil, Conductive Yellow Paint, and Gold Samples from Day of Launch..... 29

13. Diagram of RPA/TQCMs..... 36

14. Photo of ML12-6 and ML12-7 with Protective Covers Released..... 37

15. RPA/TQCM Block Diagram..... 40

LIST OF ILLUSTRATIONS (Continued)

16. ML12-6 Indicated Mass During Operations on Day 114..... 42

17. ML12 Mass Accumulation During Large P78-2 Charging in Eclipse on Day 114, 24 April 1979..... 46

18. ML12 Mass Accumulation During Quiet P78-2 Eclipse on Day 109, 19 April 1979..... 47

19. ML12-6 TQCM Mass Accumulation Rates at Various RPA Grid Bias Potentials During Winter Experiment..... 53

20. ML12-6 TQCM Mass Accumulation Rates at Various RPA Grid Bias Potentials During Summer Experiment..... 54

21a. RPA Electrometer Current Density Vs. Time in the Period Preceding and Immediately Following the AIM Burn at 21.73 Hr..... 60

21b. RPA Electrometer Current Density Vs. Time in the 2-Hr Period Commencing with the AIM Burn..... 61

22. Locations of ML12 TQCM/RPA Sensors and Hydrazine Rocket Engine Modules on the P78-2 Satellite..... 64

23. Scale Drawing of P78-2 Viewed Along Vehicle Spin Axis Showing that ML12-3, -4, and -6 Sensors Have Nearly Free Fields of View..... 67

24. Thickness of Contamination Collected on ML12-6 Temperature-Controlled Quartz-Crystal Microbalance, Assuming It Is a Uniform, Unity-Density Film..... 69

25. Plot of Change in Solar Absorptance of Fused-Quartz Mirror Vs. Thickness of Unity-Density Contamination Film, According to Theory and ML12 Flight Measurements..... 70

26. Absorption Coefficient Vs. Wavelength of Irradiated Contamination and Teflon FEP..... 71

LIST OF TABLES

1. P78-2 Experiment List..... 5

2. Summary of P78-2 Cleanliness Requirements..... 7

3. Flight Samples of Thermal Control Materials..... 14

4. Preflight Determinations of Thermal Control Coating Sample Properties..... 19

5. Parameters Giving Best Fit to Eq. (9) Along with Prelaunch Solar Absorptances Based on Spectral Measurement..... 30

6. Equilibrium Mass Accumulation Rates of ML12-6 and ML12-7 During Several Orbits in 1979..... 49

7. ML12-6 TQCM Mass Accumulation Rates at Various RPA Bias Settings..... 52

8. Correlation of ML12-6 TQCM Mass Accumulation Rates with RPA Bias Levels..... 55

9. P78-2 AIM Burn Contamination Effects on Thermal Control Coatings..... 59

SECTION I
INTRODUCTION

1. PROGRAM GOALS

During the 1970's, malfunctions of spacecraft operating near geosynchronous altitude were sometimes attributed to noise pulses generated by arcing between differentially charged members of the spacecraft. The realization of the nature of the problem grew out of on-orbit measurements of spacecraft charging,[1,2] studies of correlations between anomalous spacecraft behavior and geomagnetic conditions,[3,4] and experimental and theoretical investigations.[3-7]

Another source of difficulty with spacecraft operation, the problem of contamination of critical surfaces, was also believed to be aggravated by charging. It was argued that, in addition to line-of-sight contaminant trajectories usually considered for synchronous altitude spacecraft, a negatively charged vehicle would electrostatically reattract molecules released from the vehicle if they become photoionized while still within range of the vehicle's electric field. Such a trajectory is shown in Fig. 1. Inasmuch as the electric field from a charged vehicle can extend tens to hundreds of meters in the very dilute plasma at synchronous altitude, the molecule could arrive at almost any point on the vehicle. Theoretical estimates indicated that this mode might be important for spacecraft outgassing at typical rates, but the multitude of simplifying assumptions required in such calculations make their validity uncertain.[8,9] A major goal of ML12 was to determine if this mode of contaminant transport has engineering significance. Other goals were to: (1) determine the solar absorption and evaporative characteristics of the contamination collected on exterior spacecraft surfaces, (2) study the increase in solar absorptance of several thermal control coating materials caused by the natural space environment, (3) provide quality flight data against which the results of terrestrial and other in-space degradation and contamination experiments could be compared, and (4) identify the effects of specific contaminant releasing events such as thruster operations and boom deployments.

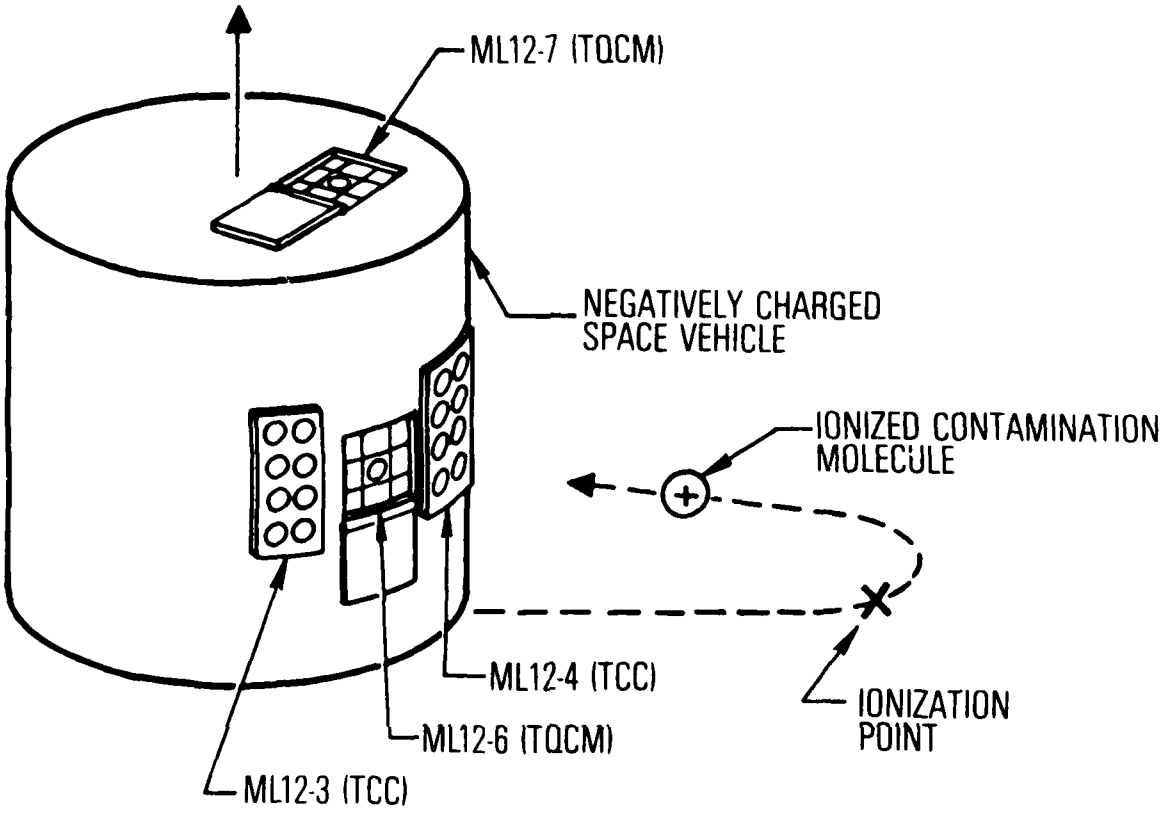

Fig. 1. Negatively Charged Vehicle Reattracting Contaminant

Although data collection and analysis is continuing, these goals have all been attained in at least a preliminary way. The purposes of the continuing efforts are discussed throughout this report.

2. SPACECRAFT DESCRIPTION

The P78-2 spacecraft is managed and funded by the United States Air Force (USAF) Space Test Program. It is one element of a cooperative National Aeronautics and Space Administration (NASA)/United States Air Force program to investigate various aspects of the electrical charging and discharging of geosynchronous spacecraft surfaces.[10] The program is known as Spacecraft Charging At High Altitudes (SCATHA).

The P78-2 was launched on 30 January 1979, into a 176- by 43,278-km transfer orbit. On 2 February, it was injected into a 27,578- by 43,288-km, 7.9-deg inclination final orbit. The vehicle (Fig. 2) is a right cylinder approximately 1.75 m in both length and diameter.

The objectives of P78-2 are to measure the environment that causes charging, the characteristics of the vehicle plasma sheath, and the effects of charging on vehicle subsystems.[4,11] It carries a complement of six charged particle experiments, electron and positive ion emitters, magnetic and electric plasma field detectors, satellite surface potential monitors, instruments to characterize electrical discharges, and the ML12 contamination experiment to achieve these objectives.[11,12] Table 1 lists the titles, principal investigators, and sponsors of these experiments.

3. OVERVIEW OF ML12 INSTRUMENTS

Two sensor types are used to accomplish the goals of the experiment. One sensor type is a combination retarding potential analyzer (RPA) and temperature controlled quartz crystal microbalance (TQCM). With it, distinction can be made between charged and uncharged arriving molecules, and information can be obtained concerning the temperature dependence of the contaminant adsorption and desorption rates. The other sensor type exposes samples of different spacecraft thermal control coatings (TCCs) to the arriving contaminants and continuously measures the solar absorptances (α_s) of these samples. Changes

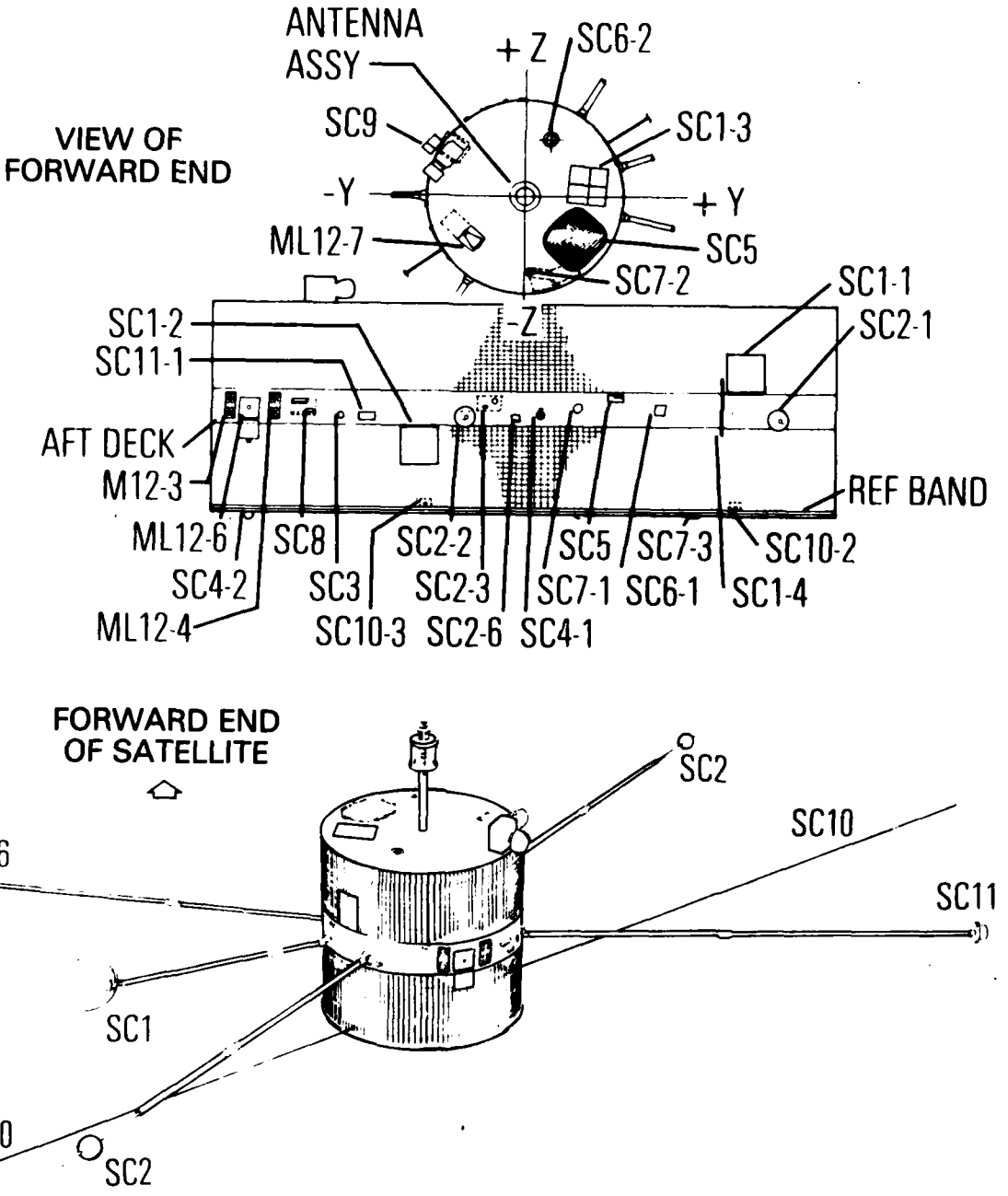

Fig. 2. P78-2 Space Vehicle

Table 1. P78-2 Experiment List

Experiment Number	Title	Principal Investigator/ Sponsor	Address
SC1	Engineering Experiments	Dr. H. C. Koons/ USAF/AFSC/SD	The Aerospace Corporation P.O. Box 92957 Los Angeles, CA 90009
SC2	Spacecraft Sheath Electric Fields	Dr. J. F. Fennell/ USAF/AFSC/SD	The Aerospace Corporation P.O. Box 92957 Los Angeles, CA 90009
SC3	High Energy Particle Spectrometer	Dr. J. B. Reagan Office of Naval Research	Lockheed Palo Alto Research Lab 3251 Hanover Street Palo Alto, CA 94304
SC4	Satellite Electron and Positive Ion Beam System	Mr. H. A. Cohen/ USAF/AFSC	Hanscom AFB/LKB Bedford, MA 01731
SC5	Rapid Scan Particle Detector	Lt. D. Hardy/ USAF/AFSC	Hanscom AFB/PHE Bedford, MA 01731
SC6	Thermal Plasma Analyzer	Dr. R. C. Sagalyn/ USAF/AFSC	Hanscom AFB/PHR Bedford, MA 01731
SC7	Light Ion Mass Spectrometer	Dr. D. L. Reasoner/ Office of Naval Research	NASA Marshall Space Flight Center Code BS-23 Huntsville, AL 35815
SC8	Energetic Ion Composition Experiment	Dr. R. G. Johnson/ Office of Naval Research	Lockheed Palo Alto Research Lab 3251 Hanover Street Palo Alto, CA 94304
SC9	UCSD Charged Particle Experiment	Dr. S. E. Deforest/ Office of Naval Research USAF/AFSC/SD	University of California B019 Dept. of Physics La Jolla, CA 92093
SC10	Electric Field Detector	Dr. T. L. Aggson/ Office of Naval Research	NASA Goddard Space Flight Center Code 625 Greenbelt, MD 20771
SC11	Magnetic Field Monitor	Dr. B. G. Ledley/ Office of Naval Reseach	NASA Goddard Space Flight Center Code 625 Greenbelt, MD 20771
ML12	Spacecraft Contamination and Thermal Control Coating Degradation	Mr. D. F. Hall/ USAF/AFSC/AFML	The Aerospace Corporation P.O Box 92957 Los Angeles, CA 90009

in α_s of space-stable samples are ascribed to contamination, whereas changes in α_s of the other samples are ascribed to a combination of contamination, photochemical, and radiation effects.

As shown in Figs. 1 and 2, there are two of each type of sensor on the satellite. Both of the TCC trays (ML12-3, ML12-4) and one of the RPA/TQCMs (ML12-6) view radially. The other RPA/TQCM (ML12-7) views axially from the "forward" end of the space vehicle. The three ML12 sensors mounted on the vehicle equatorial band between the SC2 and SC11 booms have a nearly clear field of view. The fourth sensor, mounted flush with the forward end of the vehicle, has a portion of the main communication antenna within its field of view.

In later sections, these instruments are described in more detail, and the results to date are presented.

4. SPACECRAFT CLEANLINESS REQUIREMENTS

The P78-2 program cleanliness requirements are summarized in Table 2. They are fairly typical of recent Air Force space vehicle programs, although some past programs have had more severe formal requirements while others have had less severe requirements. However, it is likely that P78-2 was cleaner than most spacecraft because the need for vehicle cleanliness was stressed from the inception of the program through launch.

Thruster operations and appendage deployments represent transient sources of contamination that could have affected the TCC samples. As shown in Fig. 3, there are two clusters of four hydrazine thrusters, known as rocket engine modules (REMs), located at the lower periphery of the vehicle. The tangential thrusters were used to change the angular velocity of the vehicle, whereas the thrusters parallel with the axis of rotation are used in a pulsed mode to adjust the angle that the vehicle axis forms with the sun line. These thrusters[21] and the results of contamination measurements made during their operation[22] are discussed elsewhere.

Table 2. Summary of P78-2 cleanliness requirements

Restricted Item	Restriction
Materials of Construction	≤ 0.1% volatile condensable materials (VCM); ≤ 1% total weight loss;[13,14] space qualified.
Surface Contamination	Components: Free of all visible contamination.[15] Vehicle witness plate before installation of launch vehicle fairing: Level 500A.[16]
Environment	Assembly and test areas: Class 100,000.[14,17,18]
	Eastern Test Range Spin Test Facility and gantry[19] areas: HEPA filtration of inlet air to remove 99.9% of particles over 0.3 μm.
	Launch vehicle fairing.[20]

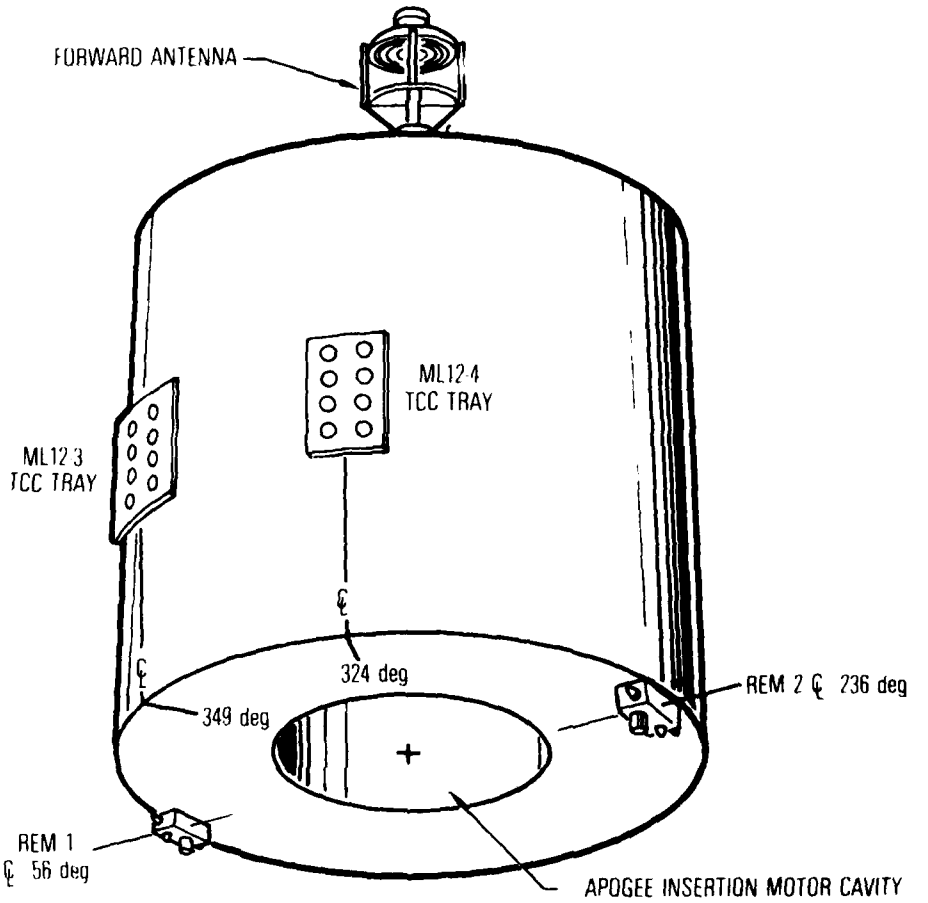

Fig. 3. P78-2 Spacecraft (booms not shown) with Locations of TCC Trays, Hydrazine Rocket Engine Modules (REM), and Apogee Insertion Motor Cavity

Also shown in Fig. 3 is the cavity that contained the solid propellant apogee insertion motor (AIM). The AIM injected the vehicle into final orbit and was ejected from the vehicle 1-2/3 days later (on Julian day 35 of 1979). No observable contamination was traced to the firing of the AIM.[23]

Five folded booms carrying sensors of other experiments were deployed during the early weeks on orbit. Also deployed were some instrument covers and two 50-m unfurlable tubular antennas. No correlation has been noted between these transient events and α_s values.

SECTION II
THERMAL CONTROL COATINGS EXPERIMENT

1. INSTRUMENT DESIGN

The thermal control coatings experiment consists of three interconnected units designated ML12-3, ML12-4, and ML12-5. These units are modifications and augmentations of hardware originally designed and fabricated at TRW Systems.[24] The ML12-3 and ML12-4 are sample trays that each carry eight 1.25-in. diameter samples. The ML12-5 carries the electronic circuitry required to monitor the TCC coupons. The location of the trays on the P78-2 vehicle is shown in Figs. 1 and 2.

The flight trays, one of which is shown in Fig. 4, were installed on P78-2 in mid-November 1978 at the Eastern Test Range and, therefore, were not exposed to possible contamination during the thermal vacuum testing of the vehicle. (With the exception of the Grafoil, paint, aluminum, and tape mounted fabric samples, the flight samples were not exposed to the thermal vacuum testing of the trays.) The dust covers, shown removed in Fig. 4, remained on the trays almost continuously until a few hours before launch, when they were removed through a special door in the space vehicle fairing.

On the trays, each test sample is mounted on an aluminum disk (Fig. 5) by means of diluted Eccobond EC57C conducting epoxy (except for the fabric/tape sample, which did not require additional adhesive). Thermal isolation is accomplished by having the disk supported by three 0.57 in. long, 14 mil o.d. stainless steel tubes, which are thermally insulated from the base of a cup by fiberglass sleeving. The length and diameter of the instrumentation leads to the disk were also chosen to minimize conduction. The volume enclosed by the disk and cup walls is filled with a combination of multilayer and open cell polyurethane insulation. The underside of each aluminum disk carries two heaters in series and three thermistors. The heaters, which are actually strain gauges, were chosen because of their low temperature coefficient of resistance. The heaters are included for preflight calibration and for thermal desorption cleaning of six of the samples on orbit. (Hardware constraints precluded making all samples heatable on orbit.) The three thermistors span low, medium, and high temperature ranges. On one-half of the

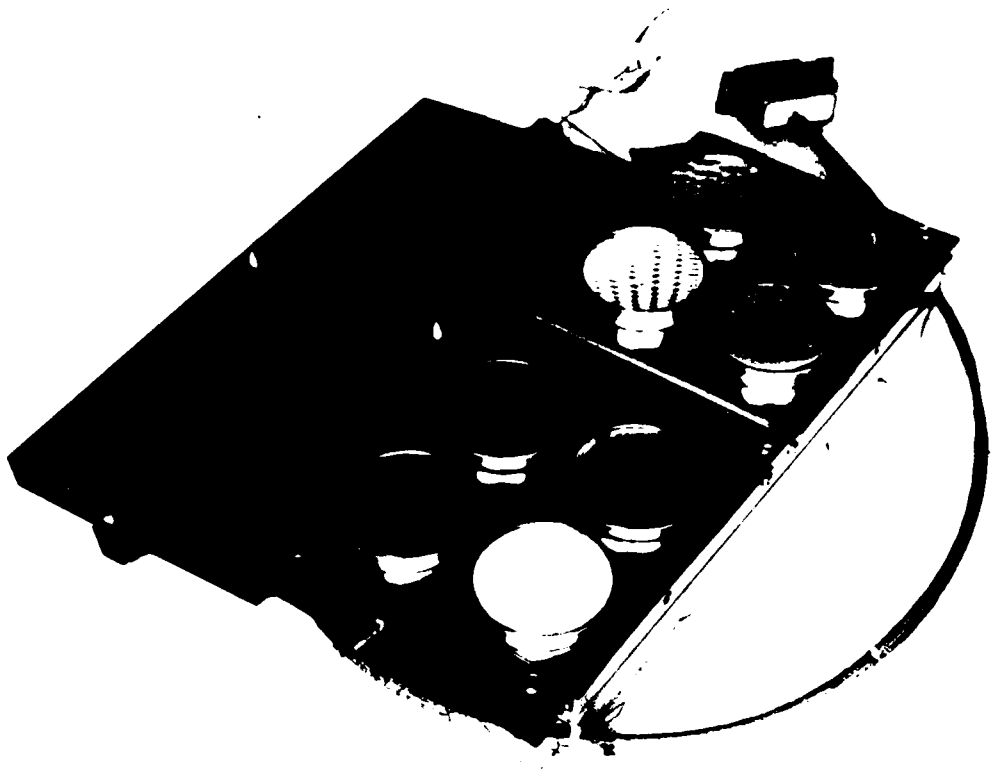

Fig. 4. Flight TCC Tray

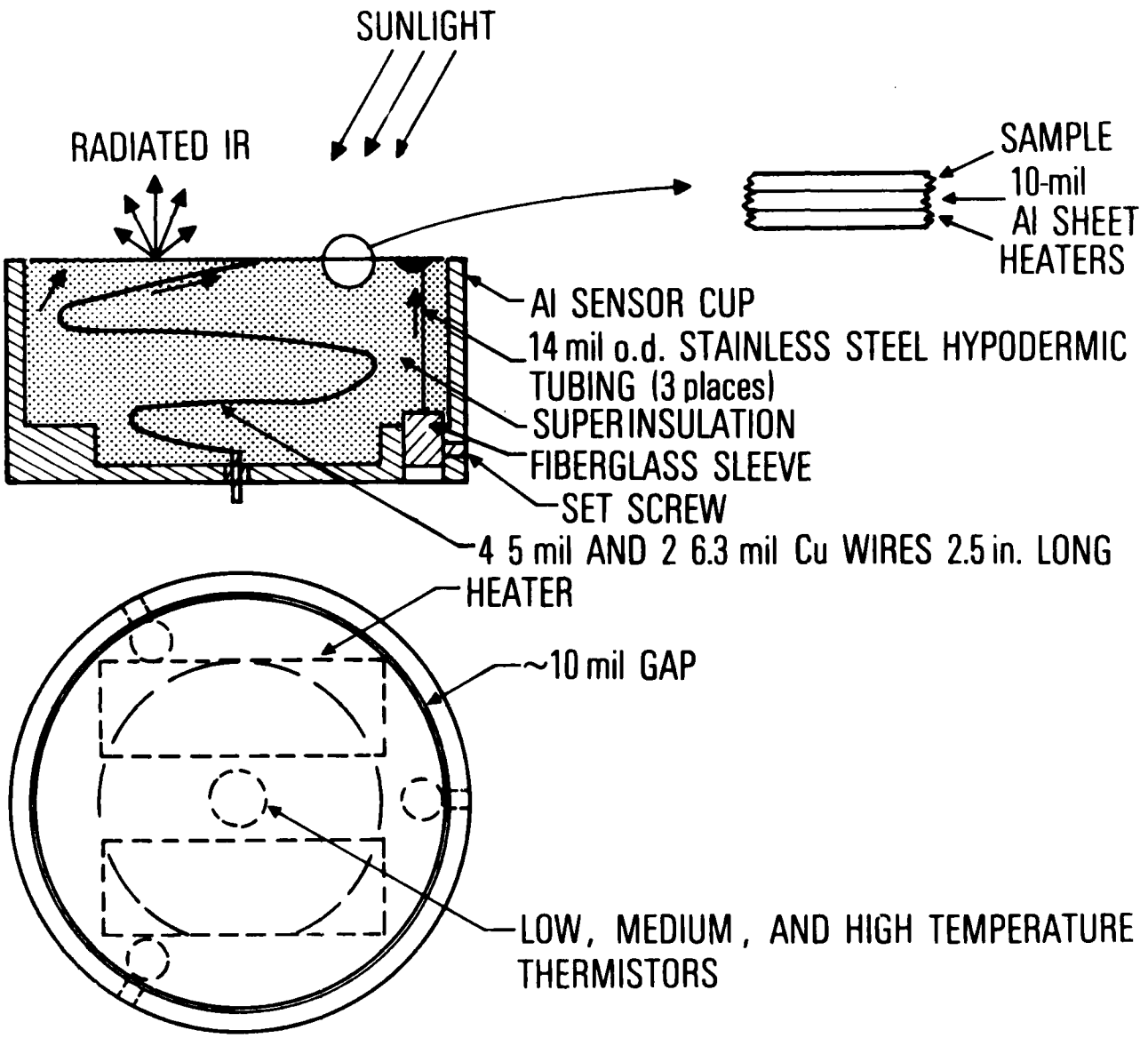

Fig. 5. Arrangement for Mounting TCC Sample Disks in Cup

samples, one of the three thermistors is monitored on the basis of the expected temperature range. On the other samples, two of the thermistors are monitored. In addition, two thermistors are located on each of the sample trays to measure the temperatures of the supporting cups.

The electronics package, ML12-5, contains ohmmeter circuits for measuring the 14 thermistors and 2 calibration resistors associated with each tray. Two stepping circuits simultaneously scan these signal sources on the two trays, dwelling for 1 sec at each source. The ohmmeter circuits convert the resistances into analog 0.0 to 5.1 V signals, which are digitized by an 8-bit digital-to-analog converter in the spacecraft telemetry system prior to recording by one of the vehicle tape recorders. Finally, ML12-5 generates, on command, a programmed heating sequence for six of the samples. This sequence consists of four heating-cooling cycles, each of which achieves a higher equilibrium temperature than the preceding cycle. The cooling cycle permits the determination of any change in α_s during the heating as a result of desorption of contaminants.

2. SAMPLE SELECTION

The 16 samples chosen for testing are listed in Table 3. These samples were chosen to:

1. Provide a wide range of initial α_s and ε_H values to facilitate contamination detection in case a given contaminant has the same α_s/ε_H as some of the substrates.

2. Include materials that are expected to be relatively space stable in the absence of contamination, such as the polished aluminum samples, the gold sample, and the optical solar reflector (OSR) sample.

3. Provide for some redundancy to permit checks for consistency. Thus, two black and two polished aluminum samples, one on each tray, were included.

4. Permit the comparison of similar materials, i.e., both the OSR and the OSR coated with a conductive In_2O_3 layer were included. Similarly, an In_2O_3-coated and an uncoated aluminized Kapton were chosen. Two thicknesses of silvered Teflon, 2 mil and 5 mil, were used. Two samples of Astroquartz fabric, one with an FEP/aluminum backing and one with an adhesive tape backing, are being tested.

Table 3. Flight Samples of Thermal Control Materials

MLL2-3 Tray	MLL2-4 Tray
Grafoil (Union Carbide, GTA Grade)	10 nm Au on 5 mil Kapton/Al (Sheldahl Lot 105788, Coated by SRI)
black Paint (3M401C10)	Astroquartz Fabric (J. P. Stevens 581)/FEP/Al
OSR (OCLI SI-100 Mirror)	In_2O_3/OSR (OCLI SI-100 Mirror)
Vacuum Deposited Au (optically opaque) on Al	22 nm 10% SnO_2, 90% In_2O_3 on 2 mil Kapton/Al (prepared by General Electric)
Diamond Polished 2024 T3 Al	Diamond Polished 2024 T3 Al
FEP (2 mil)/Ag (Sheldahl)	Black Paint (3M401C10)
FEP (5 mil)/Ag (Sheldahl)	Astroquartz Fabric (J. P. Stevens 581)/Tape (Sheldahl 405900)
Yellow Paint (NASA-Goddard No. NS43G)	Kapton (5 mil)/Al (Sheldahl)

5. Test a new material. To our knowledge, the In_2O_3/Kapton/aluminum sample had not been flown before.

6. Include samples identical to those studied in the satellite surface potential monitor package on board P78-2, which is designed to measure the amount of charging of thermal control coating samples.[11] These samples are the aluminized Kapton, the OSRs, the gold sample, the gold-coated Kapton, an Astroquartz fabric, and the 5-mil silvered Teflon.

Before delivery, all smooth samples were cleaned with a special 10% ethanol/90% trichloroethane solution on cleaning cloths purchased from Applied Research Labs.

3. DATA REDUCTION

Reduction of flight data is complicated by several facts. The sample temperatures vary as they move into and out of the sunlight during the approximately 1-min. period of revolution. The individual sample temperatures are only measured every 16 seconds. The sample temperatures are not only influenced by the α_s/ε_H ratio we wish to measure, but also by the heat interchange between the sample and its mounting hardware. The physics of this situation is represented by Eqs. (1) and (2).

$$C_v(T)\ (dT/dt) = F\left(T_c^4 - T^4\right) + C\ (T_c - T) + \varepsilon_H A\sigma\left(T_o^4 - T^4\right) + \alpha_s S\phi(t) + P \qquad (1)$$

$$\phi(t) = AE \sin \omega t \text{ for } 0 \leq \omega t \leq \pi$$
$$\phi(t) = 0 \text{ for } \pi \leq \omega t \leq 2\pi \qquad (2)$$

where

A = sample area
T = sample temperature
T_c = tray temperature
T_o = temperature of surroundings
F,C = thermal coupling constants between the sample and tray

$\varepsilon_H A\sigma$ = hemispherical emittance times sample area times Stefan-Boltzmann constant

$C_v(T)$ = heat capacity of samples

$\phi(t)$ = radiant power falling on sample

ω = angular velocity of spacecraft

E = solar irradiance

α_s = solar absorptance

S = factor between 0 and 1 to account for shading resulting from spacecraft booms

P = power applied by means of sample heater

t = time.

Albedo and earth emission are expected to be negligible at near synchronous orbit and were not included in Eq. (1). It is necessary, however, to use the appropriate solar irradiance value E for the day of the data evaluated, since this value varies approximately 7% between perihelion and aphelion.

Under normal space conditions, $P = T_o = 0$. The solution of this equation is then given by

$$T = T_{ind} + \Delta T \tag{3}$$

where T_{ind} is the solution of the time-independent equation

$$F\left(T_c^4 - T_{ind}^4\right) + C(T_c - T_{ind}) - \varepsilon_H A\sigma\left(T_o^4 - T_{ind}^4\right) + \alpha_s SAE/\pi = 0 \tag{4}$$

and ΔT is time dependent and given by

$$\Delta T = -\gamma + \left[\gamma\beta/(1 - e^{-\beta})\right]e^{-(\beta\theta/\pi)} + \gamma\beta\left[(\beta/\pi)\sin\theta - \cos\theta\right], 0 \leq \theta \leq \pi$$

$$\Delta T = -\gamma + \left[\gamma\beta/(1 - e^{-\beta})\right]e^{-(\beta\theta/\pi)}\, e^{\beta},\ \pi \leq \theta \leq 2\pi \tag{5}$$

where

$$\theta = \omega t$$

$$\beta = \pi \left[C + 4T_{ind}^{3} \left(F + \varepsilon_H \sigma A\right)^{-1}\right](C_v \omega)^{-1}$$

$$\gamma = SEA\ \alpha_s / \beta C_v \omega$$

Flight values of α_s were calculated from T_c and T by the following procedure: (1) Take $\Delta T = 0$ and $T_{ind} = T$ (i.e., the measured instantaneous value); (2) Calculate α_s from the time-independent equation [Eq. (4)]; (3) Calculate ΔT with above value for α_s; (4) Calculate $T_{ind} = T - \Delta T$ with above value for ΔT; (5) Return to step 2. ε_H is explicitly assumed constant in these calculations; values measured before flight are used.

4. PREFLIGHT CALIBRATIONS AND CALCULATIONS

The use of Eqs. (4) and (5) to calculate α_s requires calibration of each of the sample and tray thermistors; determination of the thermal coupling constants, C, F, and $\varepsilon_H A$; measurement of the heat capacity C_v of each sample; and calculation of the shading factors S as a function of spacecraft orientation with respect to the sun.

The 24-sample and 4-tray thermistors were calibrated against precision copper constantan thermocouples (two per tray) by placing the trays in a commercial temperature-regulated oven/refrigerator and by recording resistances and temperatures over the range of 203 to 388 K. The data were fitted to the equation

$$T = \sum_{i=0}^{4} C_i \left(\ln R\right)^i \tag{6}$$

where

T = thermistor temperature in K

R = thermistor resistance

C_i = power series coefficients

by a least squares routine. The standard errors of the fits varied between 0.05 and 0.27 K; all but three of the 28 values were less than 0.13 K. In comparison, the resolution of the spacecraft telemetry system yields an uncertainty of ±0.5 K.

The determinations of C, F, $\varepsilon_H A$, and C_v were performed in an ion pumped vacuum chamber containing a liquid nitrogen cooled shroud surrounding the trays. The shroud was painted black to ensure proper radiative coupling between it and the samples. The trays were held in a temperature-controlled aluminum holder and kept near room temperature to duplicate the conditions expected on orbit. Under these conditions, $\phi(t) = 0$, and $T_o = 77$ K [Eq. (1)].

The thermal coupling constants, C, F, and $\varepsilon_H A$, were determined by applying a measured amount of current to the sample heaters and by measuring the equilibrium temperatures T and T_c. Five sets of data were generated at five different power levels that were used to obtain C, F, and εA from Eq. (1). A least squares technique was used, with P and T as the variables and T_c as a known constant. The values of ε_H, as determined by this procedure, are given in Table 4.

The error in the value of α_s measured on orbit, resulting from the uncertainties in this calibration, which will be denoted $\Delta\alpha_{s,c}$, can be estimated as follows: Normally, under space conditions, $P = 0$, and $\phi(t) \neq 0$ in Eq. (1), whereas during calibration, $P \neq 0$ and $\phi(t) = 0$. Thus, P plays the same role during calibration that $\alpha_s \phi(t)$ plays on orbit. In space, $\phi(t) = 0.342$ watts. Therefore,

$$\Delta\alpha_{s,c}/\alpha_s \approx (\overline{\Delta P^2})^{1/2}/0.342\ \alpha_s \tag{7}$$

and

$$\Delta\alpha_{s,c} \approx (\overline{\Delta P^2})^{1/2}/0.342 \tag{8}$$

where $\overline{\Delta P^2}$ is the average value of the square of the uncertainty ΔP in the least squares fit. The values of $\Delta\alpha_{s,c}$ calculated in this way are given in Table 4. These errors are found to be small compared to the telemetry quantization errors discussed below. The larger error for one of the fabric samples on tray 4 is the result of a thermistor having become defective on that sample during calibration. Scheduling limitations did not permit replacement and recalibration of this thermistor. However, the error is comparable to the error introduced because of telemetry resolution.

Table 4. Preflight determination of conductive heat leaks, C; radiative heat leaks, F; normal emittance, ε_N; hemispherical emittance, ε_H; solar absorptance, α_s; and uncertainties in the orbital determination of α_s due to calibration uncertainties, $\Delta\alpha_{s,c}$; and telemetry quantization, $\Delta\alpha_{s,Q}$.

	C, W/K	F, W/K^4	ε_N'	ε_H	α_s'	$\Delta\alpha_{s,c}$	$\Delta\alpha_{s,Q}$
				ML12-3			
Grafoil	6.58E-4	9.05E-12	0.35	0.34	0.66	0.013	0.001
Black Paint	9.81E-4	4.72E-12	0.90	0.87	0.97	0.009	0.002
OSR[a]	8.73E-4	6.01E-12	0.80	0.81	0.08	0.010	<0.0005
Au on Al[a]	7.18E-4	6.88E-12	0.02	0.03	0.21	0.010	0.001
Polished Al	7.25E-4	6.78E-12	0.03	0.05	0.14	0.009	0.001
FEP (5 mil)/Ag[a]	9.83E-4	3.70E-12	0.80	0.80	0.11	0.009	0.001
FEP (2 mil)/Ag[a]	1.01E-3	3.96E-12	0.68	0.68	0.06	0.009	0.001
GSFC Yellow	9.90E-4	2.51E-12	0.91	0.87	0.31	0.010	0.001
				ML12-4			
Au/Kapton/Al[a]	8.99E-4	5.84E-12	0.12	0.42	0.53	0.011	<0.0005
Quartz Fabric/FEP/Al	1.06E-3	2.23E-13	0.86	0.68	0.20	0.008	0.003
In_2O_3/OSR	7.93E-3	6.36E-13	0.78	0.76	0.09	0.014	<0.0005
In_2O_3/Kapton/Al	7.10E-4	9.40E-12	0.78	0.71	0.40	0.016	0.001
Polished Al	8.22E-4	5.55E-12	0.03	0.04	0.14	0.014	0.001
Black Paint	7.85E-4	5.84E-12	0.90	0.92	0.97	0.010	0.002
Quartz Fabric/Tape	9.15E-4	2.64E-12	0.85	0.60	0.19	0.012	0.016
Kapton (5 mil)/Al	7.42E-4	7.53E-12	0.86	0.81	0.48	0.010	0.001

[a]Sample replaced following thermal vacuum test.

Furthermore, the temperature of this sample on orbit is monitored by an undamaged backup thermistor. There may be, of course, sources of systematic errors in addition to that addressed here.

To determine the sample heat capacities, C_v, heater power was applied and the data were recorded in the form of temperature vs. time using 30-sec intervals. Values of dT/dt for use in Eq. (2) were calculated by fitting a parabola to seven consecutive data points (t,T) by means of a least squares routine. The derivative of the parabola at the center data point was taken as the value of dT/dt there. With dT/dt determined and with T, T_c, and P measured, Eq. (1) was solved to provide C_v as a function of temperature. The resultant heat capacities of the samples are usually between 1.0 and 2.0 J/K. The heat capacities of the 1.25 in. diam 10 mil thick supporting aluminum disk alone should be 0.45 J/K. Thus, the experimentally determined values of C_v for the sample assemblies are quite reasonable.

The shading factors, S, are a function of the angle ρ between the spacecraft spin axis and the sun, primarily because of one of the booms. Maximum shading occurs for the Grafoil and yellow paint samples at $\rho = 90$ deg and represents a 10% drop in radiation. Values of S were calculated by Systems, Sciences, and Software for $80 < \rho < 100$ deg in 1 deg steps for each of the 16 samples.[25] The samples are not shaded for ρ outside this range.

5. TELEMETRY QUANTIZATION ERRORS

The degree of error to be expected in calculating α_s has been analyzed. For each sample, the various input parameters that are used in the equations were varied by amounts equal to the resolution inherent in the 8-bit telemetry processing, and the percentage of change in each calculated value of α_s was noted. The parameters of importance are: (1) data from the first two channels that are used in converting telemetry voltage to resistance of the thermistors, (2) tray temperature, (3) sample temperatures, and (4) shading factor. The last source of error depends upon the spacecraft orientation and arises from both the 1-deg resolution of the table of shading values versus ρ and the uncertainty of the angle ρ at a given time. It has been possible to eliminate the contribution of error from boom shading by selecting data

obtained when the orientation is such that the shadows miss the sample trays. At those times, the errors are those denoted $\Delta\alpha_{s,0}$ in Table 4, and the largest contributor to these errors is the result of quantization of the tray temperature.

Prior to mounting the flight samples on the calorimeters, values of α_s and normal emittance ε_N were determined optically at the Air Force Wright Aeronautical Laboratory. The solar absorptance was calculated from sample spectral reflectance measured with a Beckman DK2 spectrophotometer fitted with a Gier Dunkle integrating sphere[26] and a 25 equal energy band approximation to the Thekaekara solar spectrum.[27] The ε_N values were obtained with a Gier Dunkle DB100 inspection instrument.[26,28] These values are labeled α_a' and ε_N' in Table 4. The accuracies of the ε_N' and α_s' measurements are approximately ±0.02 and ±0.01, respectively, except in the case of the α_s' measurements of the polished aluminum samples. In these instances, instrumental problems degraded the α_s' accuracy to approximately ±0.05. Note that there are some discrepancies between ε_N' and the values ε_H that were measured calorimetrically during calibration. These discrepancies can be attributed to a number of causes:

1. The calorimetric method yielded hemispherical emittance ε_H, whereas the optical method yielded normal emittance ε_N. For low ε materials, $\varepsilon_H/\varepsilon_N$ may reach ~1.3; for high ε materials, $\varepsilon_H/\varepsilon_N$ is as low as ~0.95.[29]

2. The calorimetric method requires heat flow through the sample. If sample conductance is low, as in the case of the two quartz fabric samples, the effective emittance will be lower than that deduced from reflectance measurements. Previous measurements[30] of quartz fabrics also revealed that $\varepsilon_H < \varepsilon_N$, although the differences were not as large as those in Table 4.

3. Less than perfect bonding between the samples and the supporting disks would also lead to a reduced thermal conductance and thus affect the calorimetric determination of ε_H.

4. Samples with high surface roughness often are found to have a smaller value for $\varepsilon_H/\varepsilon_N$ than is usual. The two quartz fabric sample surfaces are quite rough.

5. Partial loss of the gold overcoat probably occurred on the gold-on-Kapton sample. Visual inspection at the time of calibration revealed that this sample was not uniform in appearance. Schedule constraints did not allow for the replacement and recalibration of this sample.

6. FLIGHT RESULTS

Plots of sample $\alpha_s(t)$ on orbit are presented in Figs. 6 through 12 as individual data points. In addition, a curve representing the least squares fit of the equation

$$\alpha_s(t) = \alpha_s(o) + Kt + \Delta\alpha\,(1 - e^{-t/\tau}) \qquad (9)$$

to the data is plotted as a continuous curve. The scatter of the data points about the fitted curve is within the range of the calculated random errors, $\Delta\alpha_{s,Q}$. The data points scatter evenly above and below the curves. Thus, it is unlikely that a better equation could be found to fit the data. The parameters of the equation for each sample, along with the preflight measurements of the solar absorptance, α_s', and the average sample temperatures on orbit, are given in Table 5.

Comparison with Prelaunch Measurements of α_s

The initial orbital values of solar absorptance, $\alpha_s(o)$, can be compared with the prelaunch values α_s' in Table 5. When measurement errors are considered, $\alpha_s(o)$ and α_s' agree for all but one of the black paints. Since all 16 samples were exposed to the same environments from the time the calorimeters were mounted on the trays, it is concluded that any contamination acquired in tray calibrations, testing, and launch was not sufficient to affect any of the $\alpha_s(o)$ values measurably. The apparent decrease in the black paint sample $\alpha_s(o)$ on ML12-3 is likely the result of a problem in the flight instrumentation, since the 0.90 value is lower than expected and not confirmed by the sample of the same paint on ML12-4.

Absorption of Contaminants

The best monitor for the influence of condensable contaminants is the uncoated OSR sample. It is the coldest sample of the group and one of the

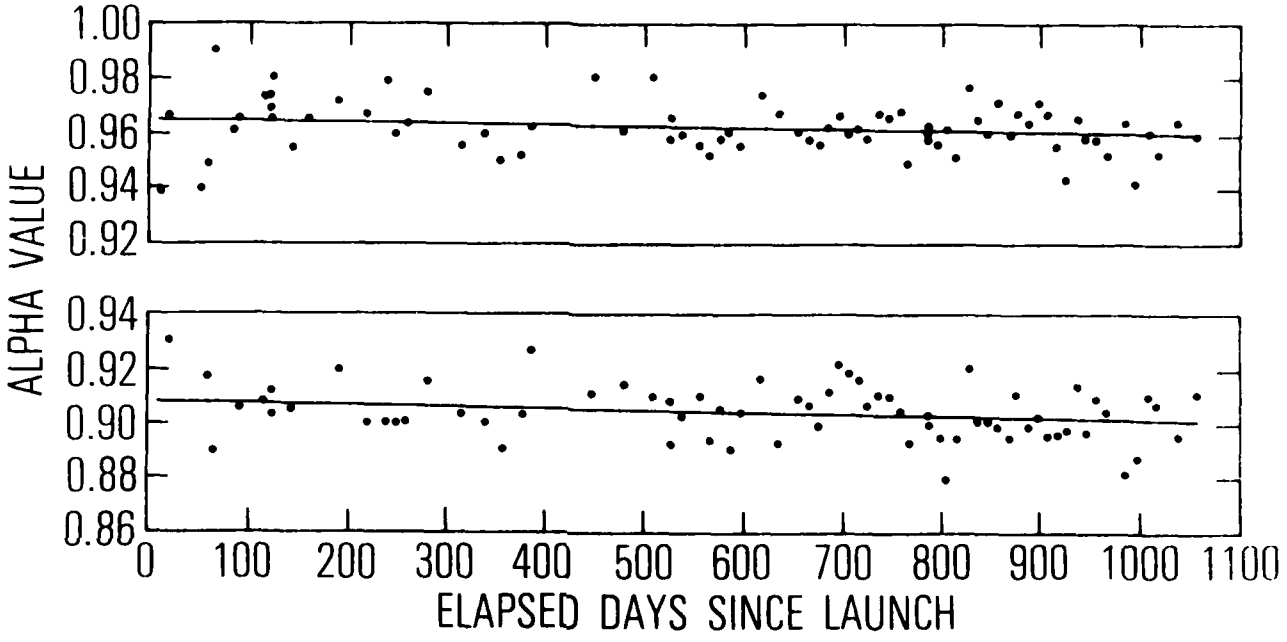

Fig. 6. Solar Absorptances of Black Paint Samples from Day of Launch

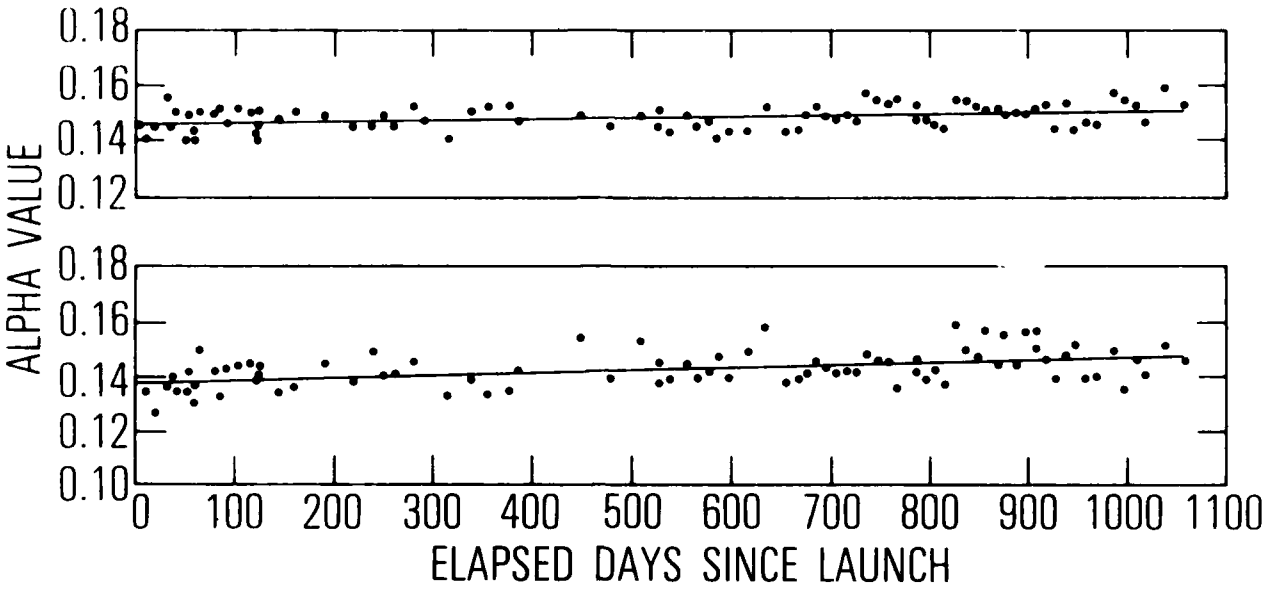

Fig. 7. Solar Absorptances of Polished Aluminum Samples from Day of Launch

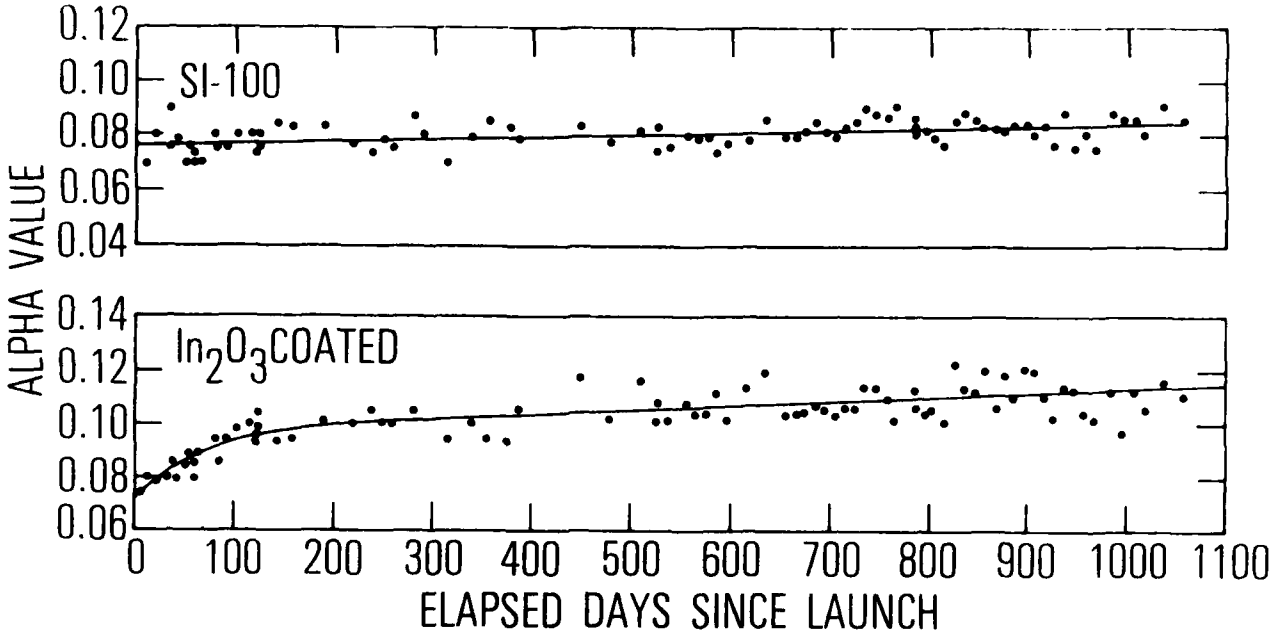

Fig. 8. Solar Absorptances of Standard and In_2O_3-Coated Fused-Silica Mirror Samples from Day of Launch

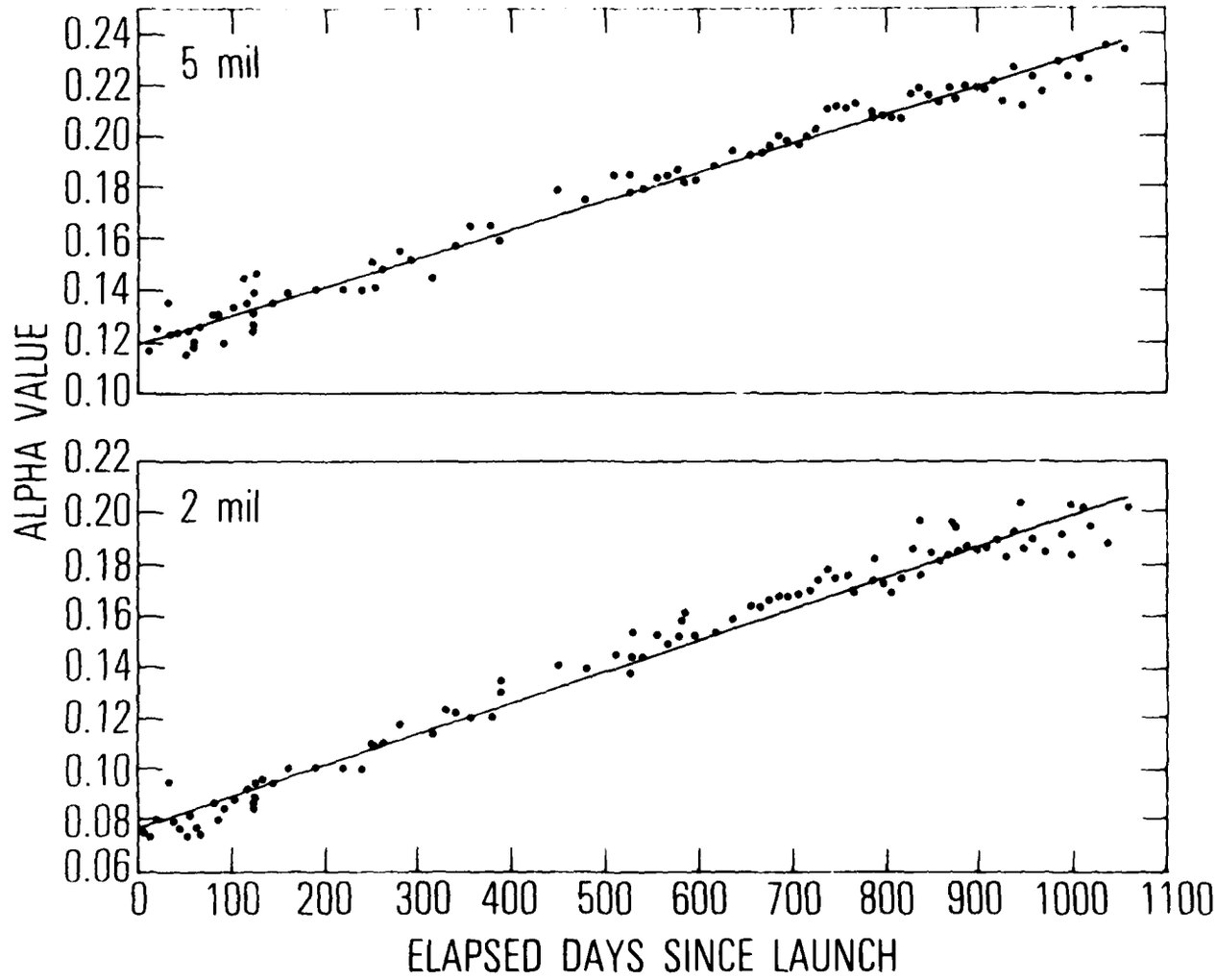

Fig. 9. Solar Absorptances of 2- and 5-Mil Thick Silvered FEP Teflon Samples from Day of Launch

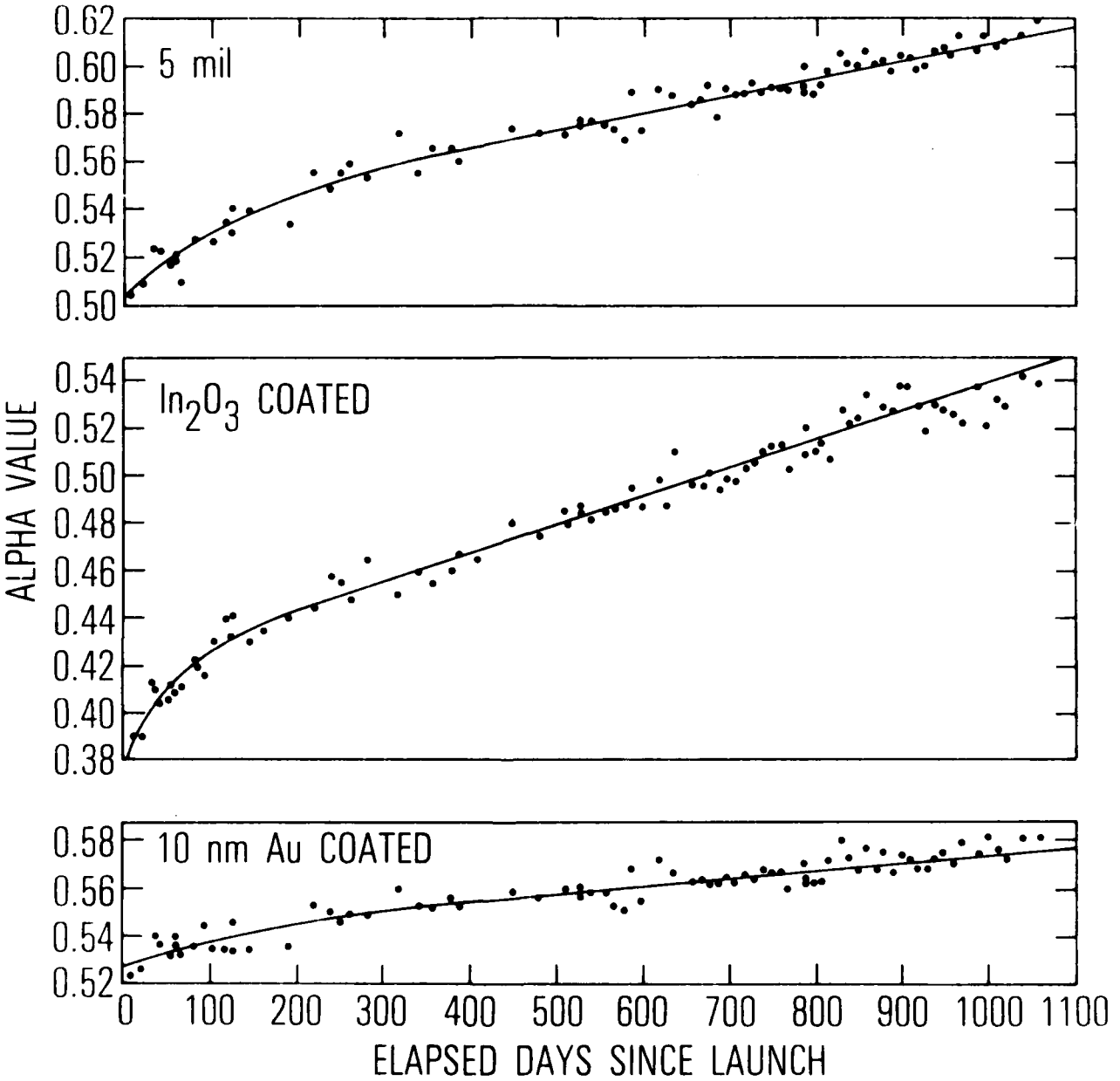

Fig. 10. Solar Absorptances of Plain, Gold-Coated, and In_2O_3-Coated Aluminized Kapton Samples from Day of Launch

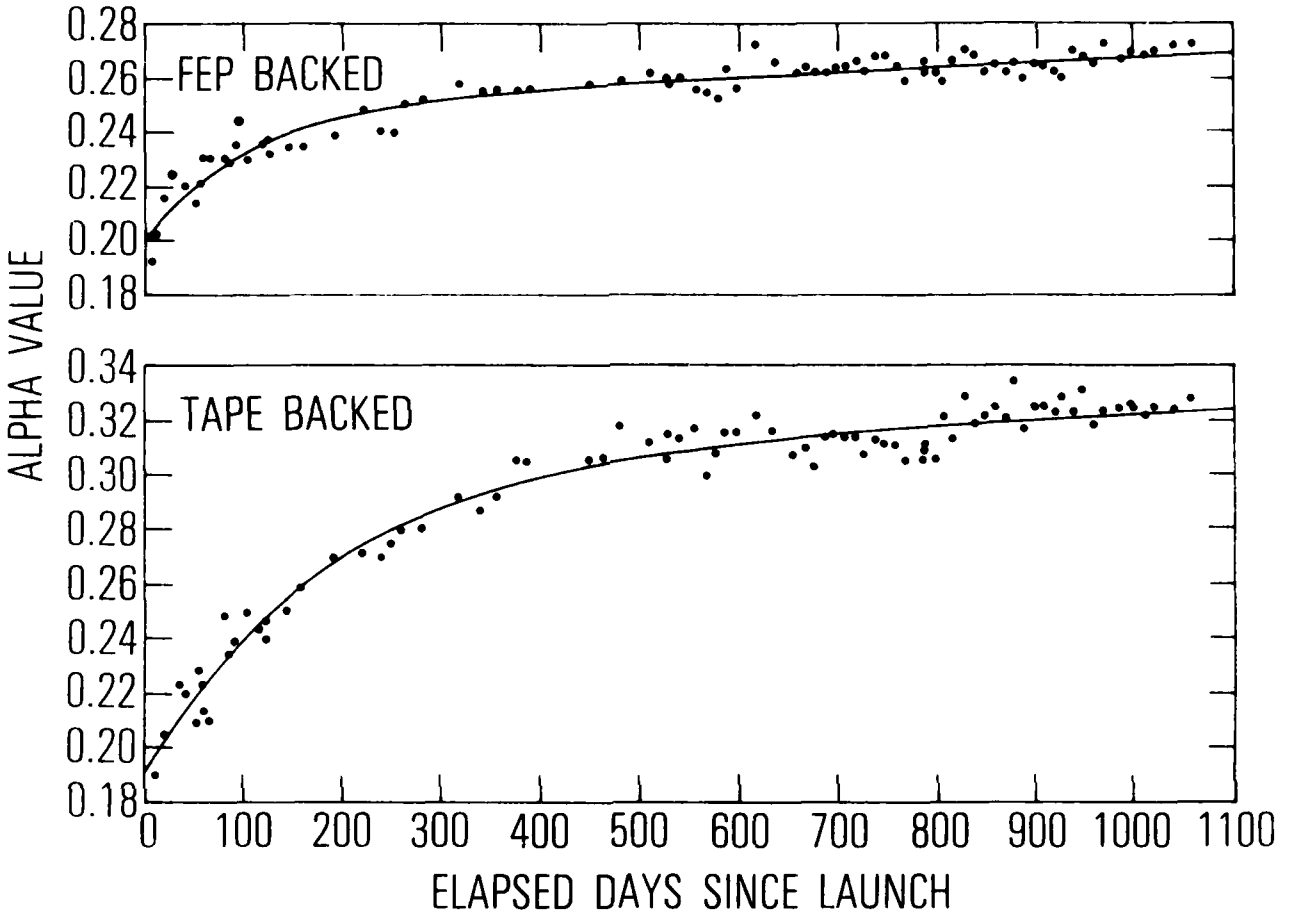

Fig. 11. Solar Absorptances of Astroquartz Fabric Samples Backed with Silvered-FEP Teflon and Double Adhesive Tape, Respectively, from Day of Launch (Day 30)

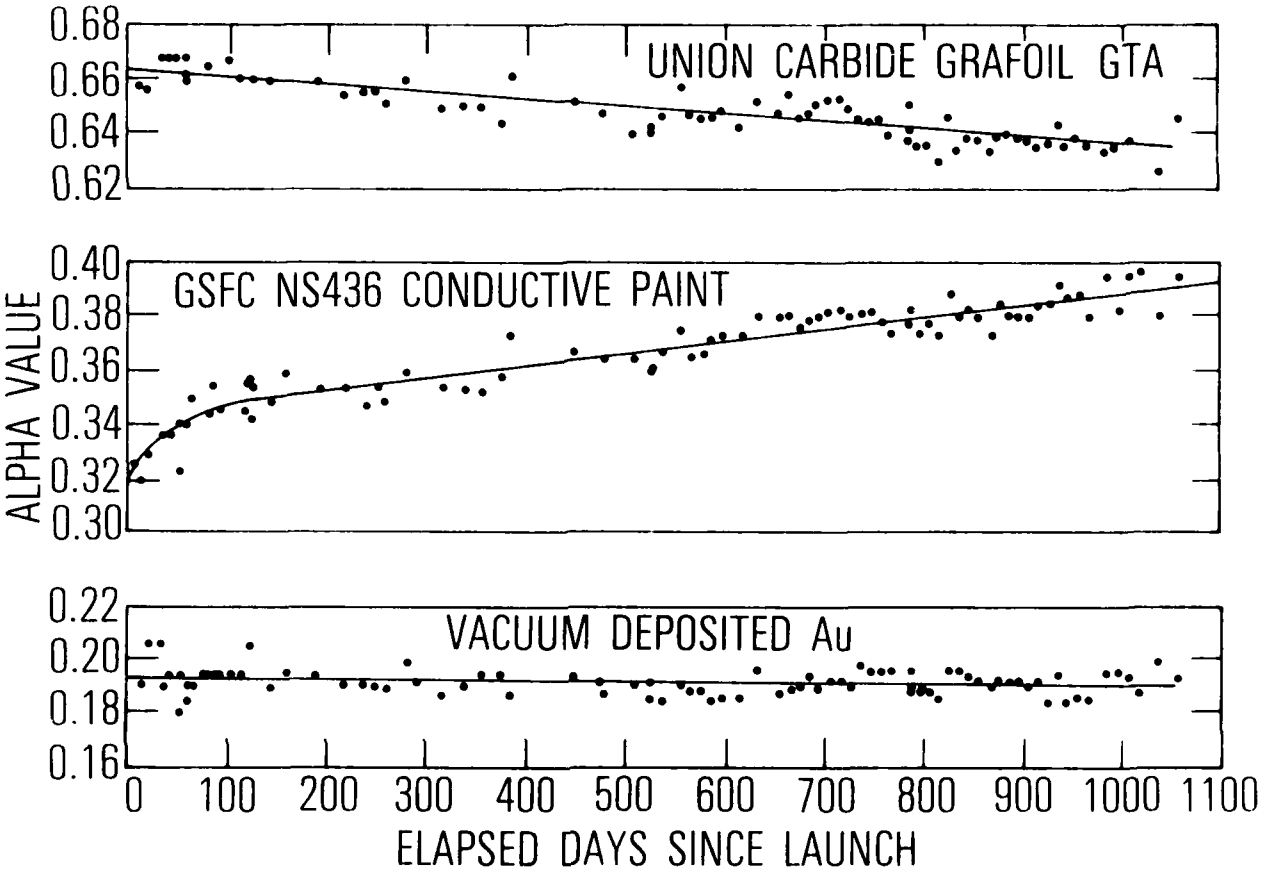

Fig. 12. Solar Absorptances of Grafoil, Conductive Yellow Paint, and Gold Samples from Day of Launch

Table 5. Parameters giving best fit to Eq. (9), along with prelaunch solar absorptances, α'_s, based on spectral measurement

Material	Typical Orbital Temperature (K)	α'_s	$\alpha_s(o)$	K ($year^{-1}$)	$\Delta\alpha$	τ (days)
Grafoil	331	0.66 ±0.01	0.66	-9.77E-3	0	--
Black Paint	301	0.97 ±0.01	0.91	-2.81E-3	0	--
OSR	234	0.08 ±0.01	0.08	2.45E-3	0	--
Au or Al	329	0.21 ±0.01	0.19	-0.67E-3	0	--
Al	315	0.14 ±0.05	0.15	1.06E-3	0	--
FEP(5 mil)Ag	242	0.11 ±0.01	0.12	40.90E-3	0	--
FEP(2 mil)/Ag	246	0.06 ±0.01	0.08	44.56E-3	0	--
GSFC Paint	260	0.31 ±0.01	0.32	15.91E-3	0.028	39
Au/Kapton/Al	312	0.53 ±0.01	0.53	11.85E-3	0.015	146
Fabric/FEP	257	0.20 ±0.01	0.20	6.65E-3	0.049	102
In_2O_3/OSR	238	0.09 ±0.01	0.07	5.47E-3	0.026	63
In_2O_3/Kapton/Al	278	0.40 ±0.01	0.38	44.12E-3	0.040	52
Al	314	0.14 ±0.05	0.14	2.76E-3	0	--
Black Paint	300	0.97 ±0.01	0.97	-2.11E-3	0	--
Fabric/Tape	267	0.19 ±0.01	0.19	6.70E-3	0.115	183
Kapton(5 mil)/Al	282	0.48 ±0.01	0.50	25.49E-3	0.036	127

least likely to experience material degradation. The very small rise in α_s for this sample, amounting to 2.5×10^{-3} year^{-1} and representing an upper limit for contaminant effects, indicates that contamination was minimal and that P78-2 was a fairly clean spacecraft. This is discussed in Section 1.4. Note that the changes in α_s of the two aluminum samples and the gold sample are also quite low. The large changes in α_s observed on other samples must then be considered to result from material degradation.

Degradation of the In_2O_3 Conductive Coating

A nearly transparent In_2O_3 coating was carried on two of the samples: a fused silica mirror and an aluminized Kapton sample. This coating is electrically conductive, and when it is properly connected to the spacecraft frame it should prevent these dielectrics from acquiring a large electrostatic charge during the magnetic substorms that occasionally occur at synchronous altitude. (No attempt was made to ground the coating on these samples in this experiment. Therefore, the surfaces may charge and affect the kinetic energy of arriving charged particles just as with uncoated samples.) Comparison of the $\alpha_s(t)$ curves of the conductively coated samples with their uncoated counterparts indicates that the coating is responsible for a higher degradation, which consists of both short-term and long-term components.* The former has a time constant of approximately 2 months. This degradation is greater in the Kapton sample than the OSR.

Degradation of the Kapton Samples

Comparison of the data for the three Kapton samples also provides evidence that material degradation of the polymer is responsible for the large changes in solar absorptances. The gold-coated sample shows the smallest change in α_s, and is the sample whose α_s would be the least affected by the properties of the Kapton.

*Data collected subsequent to those shown in Fig. 8 and summarized in Table 5 indicate that the values of K for the coated and standard OSR samples agree within the statistical uncertainties of the two measurements.

Degradation of the Silvered Teflon Samples

These two samples degrade similarly in magnitude and time dependence in spite of their different thicknesses. One explanation is that the degradation is induced by low-energy radiation and extends less than 2 mil from the surface. This is consistent with our knowledge of the radiation environment at synchronous altitude and the penetration depth of this radiation as discussed below.

Degradation of the Astroquartz Fabric Samples

The most severe degradation of these materials occurred over the first 2 years. Note that the long-term changes in α_s, as parameterized by the value of K, are nearly identical for the two samples. These values are more than twice that of the uncoated OSR, and are probably attributable to condensable contaminants; the greater effect on the fabrics is caused by their greater surface area.

When we consider the transient degradation, the much higher change in α_s for the tape-backed sample indicates that the backing material is a major source of difficulty with these fabrics.

Degradation of the Paints and Grafoil

There may have been some bleaching of the two black paint samples, but this is uncertain because of the large amount of scatter in the data. The Grafoil sample, on the other hand, exhibits unequivocal bleaching. The Goddard paint displays both a transient and a long-term degradation.

Comparison with Other Experiments

Our data indicate that P78-2 was an exceptionally clean spacecraft. The field of view of our calorimeters, except for two booms, was devoid of line-of-sight contaminant sources. Most data published from other spacecraft exhibit much higher changes in the solar absorptions of the TCCs and even of OSR samples. For example, $d\alpha_s/dt$ for the OSRs on board three COMSTAR satellites[31] fell in the second year on orbit to values between 0.012 and 0.021 per year. These are still 5 to 10 times greater than we observed on P78-2. Other flight data exhibit similarly higher rates of change for these and other

samples. In contrast, data on the change in α_s for silvered Teflon and OSRs on one clean operational satellite are comparable to those reported here.[32] Contaminants from an outgassing spacecraft will obscure the material degradation contribution of the change in α_s, so direct comparison to most flight data is difficult.

It is fruitful to compare our flight data with ground measurements, even though providing good simulations of the space environment is exceedingly difficult. For instance, the degradation rate of the silvered Teflon FEP samples is approximately independent of sample thickness. This indicates that low-energy radiation damage is important. Bourrieau and Paillous also assumed low energy in a theoretical treatment of radiation damage in polymers and developed a model consistent with an extensive body of ground simulation data.[33]

The high rates of degradation for the two quartz fabrics and the conductive paint coatings are frequently observed in both flight and terrestrial experiments. In particular, the fabric performance is quite similar to samples flown at much lower altitude on the P78-1 vehicle.[34]

7. SUMMARY

With one exception, the early orbital values of α_s are in good agreement with prelaunch values obtained from optical reflectance measurements. Apparently, little contamination was acquired by the samples during launch and prelaunch activities.

Temporal data have been presented for the 16 TCC samples over 3 years on orbit. Because the satellite spins, π hours are required to accumulate one equivalent sun hour. Of course, sample property changes resulting from vacuum and energetic particle bombardment effects are not "slowed" in this way. However, contamination-related change may be slowed because of sunlight effects on contaminant adhesion[35] and optical properties.[36]

Measurements on the space-stable samples, and on the uncoated OSR sample in particular, reveal that contamination by condensable materials was minor on P78-2 and contributed an α_s change of less than 0.00245 yr^{-1}. Thus, except for the fabrics, the large changes observed on other samples have been attributed to degradation of the material itself.

In the case of the second surface mirrors, silvered Teflon and aluminized Kapton, damage by radiation of low energy and short penetration seems to be responsible for the change in α_s. The additional degradation of the In_2O_3 coating on two of the samples may also be due to this mechanism.

The two Astroquartz fabric samples on board P78-2 both showed large changes in α_s. Our data indicate, however, that the problem resides in the optical or thermal properties of backing material and the propensity for the fabric to acquire prelaunch contamination.

Within a large margin of error, the black paint samples exhibited little change. However, at Goddard Space Flight Center conductive paint has both transient and long-term degradation.

Since the degradation of most of the TCC samples has not yet indicated signs of saturation, and since most future AF satellites in high earth orbit will be expected to function for 7 to 10 years, there is obviously great motivation to continue to collect and analyze data on these samples.

SECTION III
RETARDING POTENTIAL ANALYZER/TEMPERATURE CONTROLLED QUARTZ CRYSTAL MICROBALANCE EXPERIMENT

1. INSTRUMENT DESIGN

The RPA/TQCM construction is shown in Fig. 13. Figure 14 is a photograph of the flight hardware. The RPAs were designed and fabricated at The Aerospace Corp. The TQCM sensors were supplied by Faraday Laboratories, La Jolla, California.[37] The TQCM sensor has a field of view of approximately 2.24 Sr (50-deg half-angle cone), and the RPA has a coaxial field of view of approximately 3.5 Sr (59-deg half-angle cone).

The TQCM sensors are two AT-cut, 15-MHz, optically-polished crystals with aluminum electrodes. The AT crystallographic cut minimizes the sensitivity of piezoelectric crystals to temperature change. The sensitivity is 1.6×10^{-5} g/m^2-Hz; therefore, for the ±1.0 Hz telemetry resolution and an integration time of 1 hr, the net sensitivity is approximately 1.6×10^{-5} gm^2-hr. This corresponds to the deposition of a 0.016-nm-thick uniform film of unity density per hour. Flight data indicate that the oscillator stabilities justify much longer integration times. The maximum mass loading for which the sensor crystal will oscillate is approximately 1 g/m^2.

The TQCMs are radiatively cooled but can also be operated at elevated temperatures by the use of heaters. The radiators are silvered, fused-silica, second-surface mirrors coated with electrically conducting indium oxide connected to the spacecraft ground. This coating prevents electrostatic charge buildup on the radiator surface. The TQCM sensor heaters can be commanded from the ground to maintain one of five predetermined temperatures in the range of -60 to +70°C. "Controller off" is a sixth command state, which produces temperatures of approximately -40°C in ML12-6 and about -95°C in ML12-7. Precision helium-filled, platinum resistance thermometers, which are linear to ±0.5%, indicate the TQCM temperature.

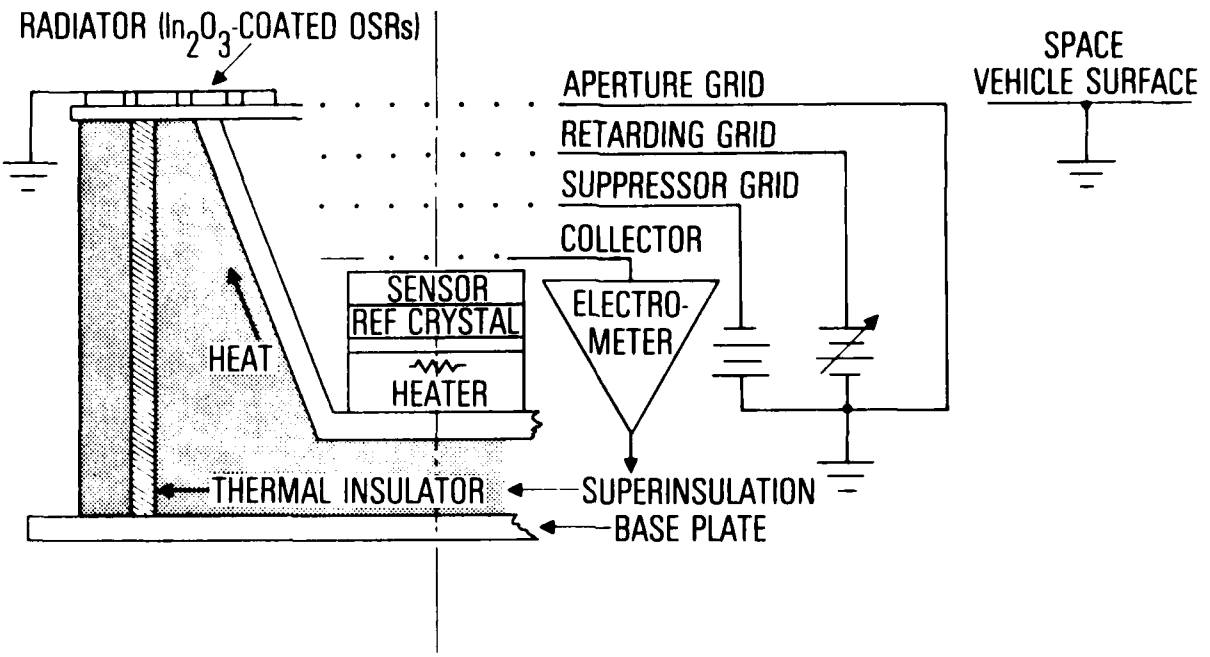

Fig. 13. Diagram of RPA/TQCMs (ML12-6 and ML12-7)

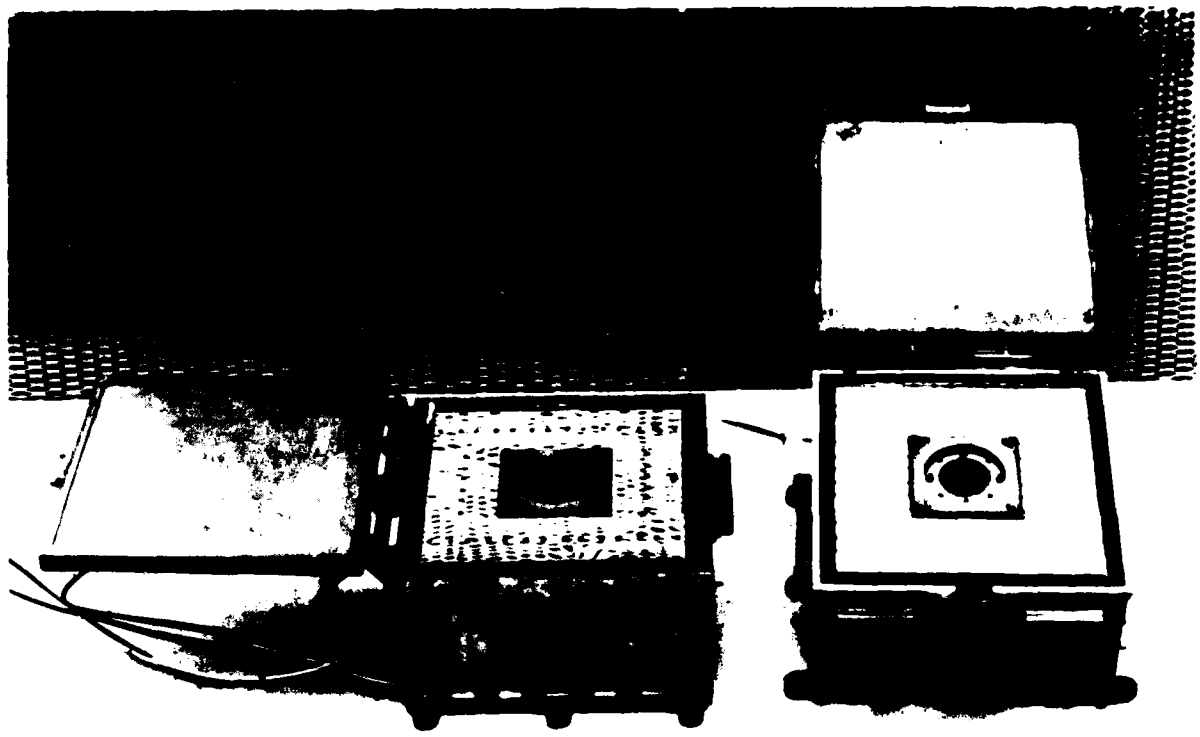

Fig. 14. Photo of ML12-6 and ML12-7 with Protective Covers Released

The TQCM receives molecules through a gridded aperture in the RPA collector. The aperture grid is normally grounded to minimize defocusing of incoming ions. Together, the four RPA grids will intercept approximately 35% of the incident contaminant flux. The flux rates quoted below have been corrected for this interception.

The retarding potential grid is commanded from the ground to one of the following potentials: +500, +100, +10, +1, 0, -1, -10, or -100 V. Alternatively, it may be commanded to cycle through these values, dwelling 8 sec at each potential.

An approximately 2-1/2 cm^2 annular collector plate (located immediately above the sensing crystal), in combination with an electrometer and guard ring circuitry, measures currents in the range of 10^{-12} to 10^{-8} A with a resolution of $\pm 10^{-12}$ A. This is approximately 6×10^{10} to 6×10^{14} electrons/m^2-sec or the equivalent in ionized condensable and noncondensable molecules.

The digital electrometer selects one of two slightly overlapping current ranges automatically, and outputs an appropriate range bit. It will also select the appropriate polarity and output a polarity bit, although it can be commanded to stay in the positive (ion) mode.

The electrometer was calibrated over the current range of 1×10^{-11} to 2×10^{-7} A. Errors in the digitized output of this circuit are created by leakage, component tolerance, and binary resolution. The least count expected of one telemetry read group is about 500 pps. Since this is subject to at least a one-bit indecisiveness, a 0.2% error can be expected from that alone. In addition, the electrometer is composed of temperature-dependent semiconductor elements, the main item of which is the field effect (FET) dual transistor (2N5907) used at the input of the electrometer preamplifier. Leakage currents in this input stage amount to an equivalent of 10 binary counts at the output, or about 5×10^{-13} A dc equivalent input at room temperature. This data offset can be of either polarity, but is more probably of the sign of a fictitious ion current at the input. Superimposed on this leakage are the effects of small unknowns, such as stray capacity and changes in the real capacitance of the 2 pF capacitor in the preamp feedback loop,

drifts of the offset voltage of the electrometer operational amplifier (a Harris HA2700), and to a lesser extent, similar drifts of the subsequent circuitry. The total of these effects has been determined during the instrument calibration, and is about equal to 20 binary counts per second or $\pm 10^{-12}$ A at room temperature.

There are essentially two kinds of connections with the spacecraft: commands and data. The commands received by the instrument are binary groups, serially received. The spacecraft system is capable of groups of larger size, but in this instance an active set of six is used. The internal instrument control of grid bias levels, polarity of the electrometer, autocycling of the grid bias generator, and the connection of the aperture grid are made possible by this command circuit.

The data outputs to the spacecraft are either serial digital or low bandwidth analog. Spacecraft telemetry-system signals are used to control both the serial digital data outputs and the serial binary command inputs.

Figure 15 is block diagram of the RPA/TQCM instrument showing the scientific (but not the housekeeping) data outputs. These outputs are labeled with their P78-2 telemetry designations as well as by function. Measurement numbers beginning with 4 are of the analog type, whereas those beginning with 8 are digital. For instance, M8001 is the digital output of the frequency counter which measures a frequency of ML12-6, whereas M4039 and M4040 are high and low sensitive analog representations of this quantity which could be used if the frequency counter fails.

The frequency counters that produce M8001 and M8002 use CMOS circuit chips. A total digital count of 2^{22} ($\simeq 4 \times 10^6$) can be stored without overload in 1 sec. This 22-bit group (with leading zeroes, if any) together with two bits of instrument status information is serially delivered to the spacecraft telemetry system once per second. Count accumulation is interrupted each second for 40 μsec while the counter data is parallel-loaded into the output shift register. These data are stored for 1 sec before they, in turn, are sent to the telemetry system. Therefore the system is responsible for a 1 sec delay in the data gathering. All the timing signals required to operate

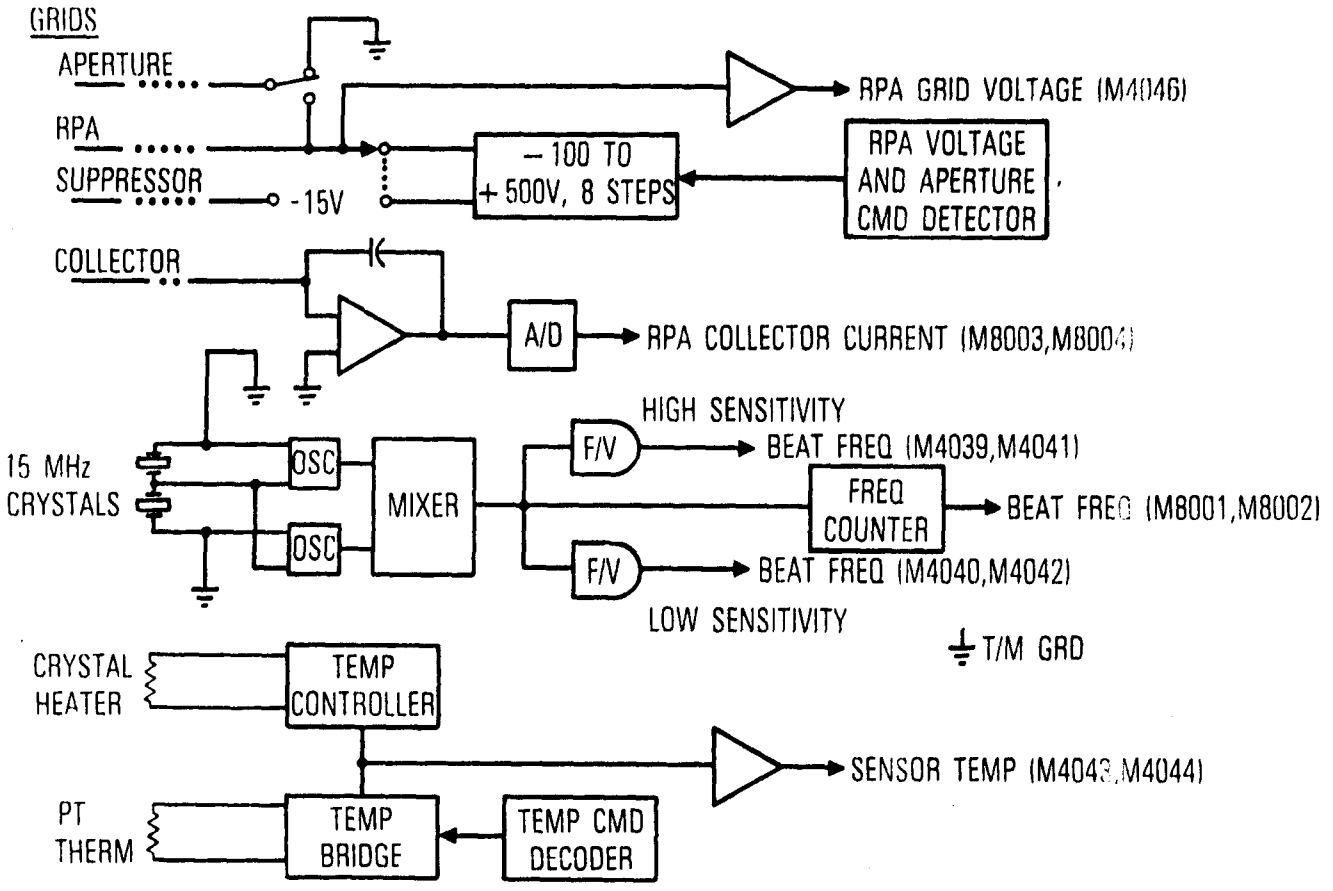

Fig. 15. RPA/TQCM Block Diagram

the circuit are received from the spacecraft telemetry system, so the absolute accuracy of the frequency counter is affected by the accuracy of the spacecraft clock.

2. DATA REDUCTION

As mentioned previously, the TQCM is a 15-MHz instrument with the sensing and reference quartz crystals in tandem. The crystal electrodes are aluminum films. The sensitivity to collected mass is 1.56 ng/(Hz cm^2) with the frequency measured as the beat frequency between the sensing and reference crystals. When the optical density of the RPA is taken into account, the mass sensitivity is 2.4 ng/(Hz cm^2). The TQCM can be commanded to "free run" (no temperature control) or to one of the following nominal temperatures: -60, -30, 0, 30, or 100°C. (In the case of the ML12-6 TQCM, temperature control occurs 7°C below the nominal set point. Because it receives heat from the sun, ML12-6 attained a temperature of about -39°C in the free run state during the first months on orbit, whereas ML12-7 fluctuated between -90 and -100°C when continuously shadowed.) Temperature is controlled with built-in heaters and energy is dissipated by means of thermal contract with indium-oxide-coated mirror radiators. The locations on the spacecraft of the two TQCM/RPA sensors, ML12-6 and ML12-7, are shown in Fig. 1.

The frequency data obtained from ML12-6 and ML12-7 share some common features. Both TQCMs have relatively small sensitivities to ambient temperature; nonetheless, a measurable change in frequency is produced when the ambient temperature is changed 30 or more degrees Celsius with a temperature command.

The TQCMs both responded strongly when sunlight fell directly on the sensing crystal. However, ever since the vehicle was placed in its final attitude, ML12-7 has been continuously shadowed and the output signal has not had large periodic fluctuations. In contrast, the ML12-6 sensor crystal is illuminated on every revolution of the vehicle.

In Fig. 16, the response of the ML12-6 sensor during Julian day 114, 1979 is shown with the time scale expanded. A solid line through the data points and a lined area corresponding to the interval in which sunlight strikes the

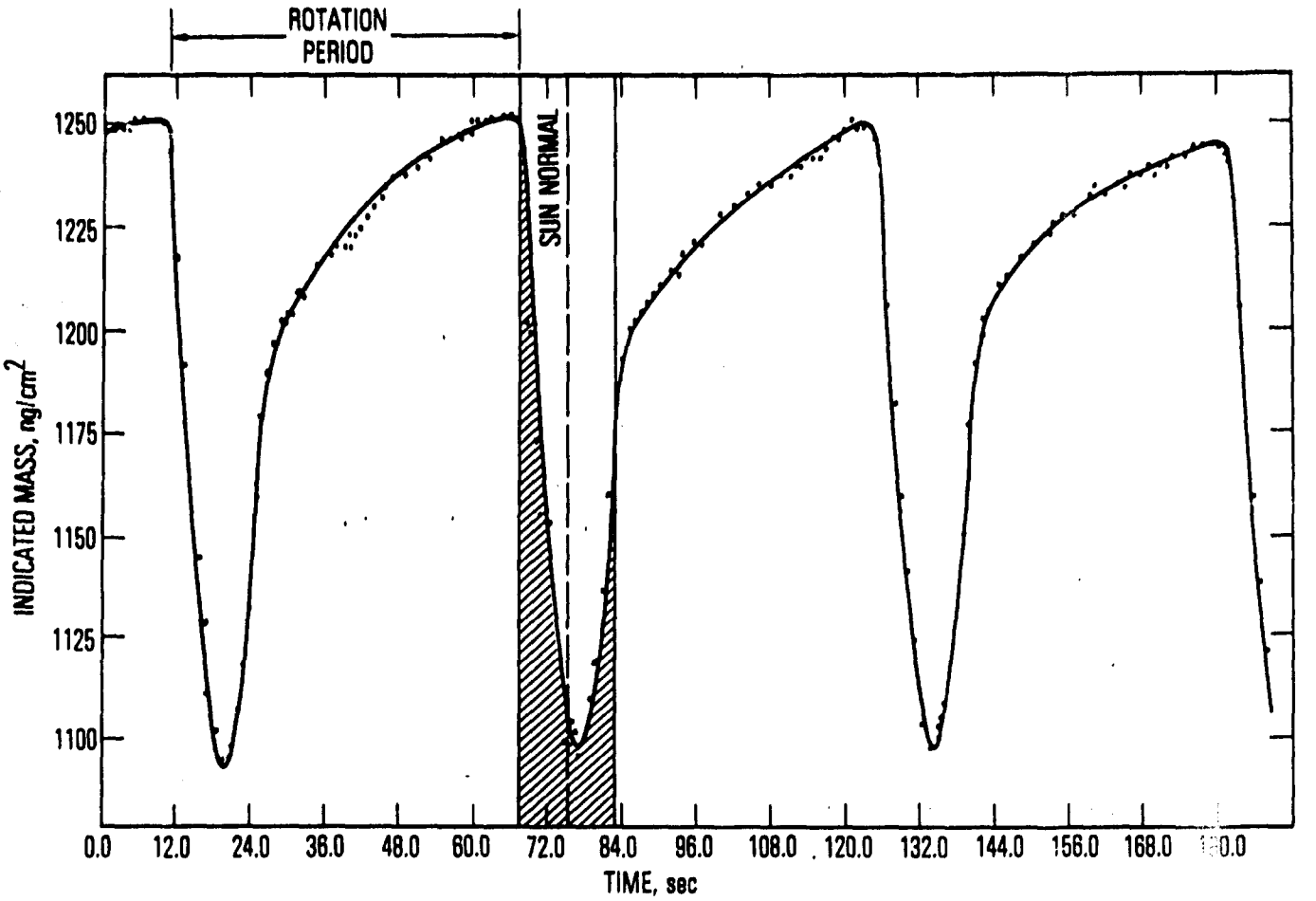

Fig. 16. ML12-6 Indicated Mass During Operations on Day 114 (24 April 1979)

sensor surface have been added for clarity. When sunlight strikes the sensor surface, the apparent mass undergoes large excursions covering approximately 150 ng/cm^2. This behavior might be the result of differential heating of the sensor quartz crystals, i.e., the reference crystal temperature remains constant while the temperature of the sensing crystal varies as a function of the amount of radiation striking the sensor. The quartz crystals exhibit a dependence of frequency upon temperature.[39] Another explanation is that the sensor frequency is affected by lateral temperature gradients in the sensing crystal induced by sunlight striking near its center. We cannot distinguish between the two possibilities without laboratory work. Such work was not undertaken, because the analyses of the flight data would not be affected by the mechanism of this frequency effect. When the spacecraft rotation causes the sensor to be shadowed following exposure to sunlight, the apparent mass value increases toward an equilibrium value. However, the sensor is exposed to the sunlight again before equilibrium is reached, leading to a new temperature cycle.

For most analyses this periodic fluctuation in ML12-6 output may be ignored. It takes many minutes to accumulate 1 Hz worth of mass on the crystal, even during periods of high deposition rate. Therefore, an occasional sampling of ML12-6 signal peak value produces a satisfactory record of mass accumulation. In those special cases where the ML12-6 output fluctuations may obscure an effect, the techniques described in Ref. 22 may be employed.

Both TQCMs suffered a change in beat frequency during launch. This was expected because changes had occurred whenever they were shake tested. It is believed that these changes were caused by displacement of the long, fine wires that connect the cold crystal assembly with the room temperature oscillators. It is well known that the frequency of crystal controlled oscillators can be "trimmed" with small capacitances across the crystal or from one lead to ground. Therefore, new "zero" mass beat frequency values had to be assigned to each instrument to avoid negative mass readings in the case of ML12-7 and unreasonably high readings in the case of ML12-6. This means that the TQCMs cannot provide data concerning mass accumulation during the launch.

3. FLIGHT RESULTS

The data set obtained from the RPA/TQCM instruments is very large. It can be used to investigate a number of different aspects of spacecraft contamination. Most of the work completed to date has been presented to the technical community at seven scientific meetings. (Papers devoted to TCC experiment results were presented at two additional meetings.) These papers are excerpted and summarized below.

Reference 40 was an invited paper prepared a few months after the P78-2 launch:

> Qualitatively, the RPA currents respond to grid voltage commands in the expected manner. For instance, when the vehicle frame is known to be negatively biased by approximately 400 V with respect to the ambient plasma potential, commanding the retarding grid to +500 V reduces the ion current recorded by the electrometer. Similarly, when the vehicle is positive, larger negative grid potentials diminish the electron current recorded. . .
>
> The continuously shadowed ML12-7 TQCM recorded mass accumulation ranged between 0 and 11 ng cm^{-2} day^{-1} during the early weeks on final orbit when its temperature was about -95°C. On March 29, 1979, its temperature was increased to -30°C, and since that date it has been commanded to temperatures between -30 and +20°C. No mass accumulated on this detector at these temperatures. . .
>
> The ML12-6 TQCM sensor, which initially was operated at about -40°C, began experiencing mass accumulation soon after final orbit was achieved. This higher temperature was reached in the case of ML12-6 with no applied heater power because the sun line is maintained between 85 and 95 deg to the vehicle spin axis. The mass accumulation rate was initially about 17 ng cm^{-2} day^{-1} and gradually diminished to approximately 12 ng cm^{-2} day^{-1} by the end of June, suggesting that the source of this material is diffusion limited. The accumulation rate was relatively insensitive to sensor temperature over the -40 to +70°C range, suggesting that either the material initially had a high desorption energy or that sunlight quickly transformed it into a material with a high desorption energy. . .
>
> Quick look, "raw" data in tabular form are available for a few brief periods (of less than 1 hr) of spacecraft charging. Enhanced accumulation rates are usually not evident from casual inspection of these data. . .

Reference 41 was solicited by the session chairman, and prepared at the end of 1979. It reported the first attempt to observe increased rate of contamination during a P78-2 charging event. The event chosen for study was the largest and longest for which data were available. As the following excerpt relates, the thermal response of the TQCMs to eclipses masked any enhancement of contamination rate caused by the spacecraft charging:

> During the earth eclipse of the sun which occurred on April 24, 1979 (Julian Day 114) the P78-2 frame was significantly charged negative for most of the 47 minute period as shown in [Figure 17]. The variation in potential observed is due to (1) disappearance of photoemission at approximately 0715 hours and its reappearance at approximately 0803; (2) temporal variations in the flux and energy distribution of ambient plasma electrons; (3) intermittent operation of the SC4-1 and SC4-2 charged particle guns in the period 0732 to 0802.
>
> The response of the ML12-7 mass detector to this event was a very small apparent increase in mass per unit time which became zero at approximately 0900 (an hour after the event was over) and then slightly negative during the next two hours. This response is believed to be an experimental artifact since it also has been obtained in eclipse where there was no charging of P78-2. Probably it arises from the sensitivity of the mass detector to temperature which probably decreases slightly during the eclipse due to cooling of the main communication antenna and mast which are within the sensor field of view.
>
> As indicated in [Figure 17] the response of the [~ 30°C] ML12-6 detector to this event initially was a rather large apparent increase in mass accumulation rate which followed an equilibrium apparent rate of approximately 16 ng/cm^2 hr. When the eclipse was over, however, the detector appeared to lose mass, rapidly at first and then more slowly. Within 1-1/2 hours of the eclipse termination, the indicated mass on the detector was identical to that before the eclipse and the accumulation rate was again nearly zero.
>
> It is believed that the M6 response to the event was also an experimental artifact rather than evidence of enhancement of spacecraft contamination rate by spacecraft charging. The reasons for our belief are as follows:
>
> If the detectors were measuring electrostatically reattracted ionized contamination, the rate should be sensitive to the large changes in space vehicle potential which occurred during the eclipse. Furthermore, a very similar response was obtained in the eclipse of March 28, 1979 (day 88), as shown in [Figure 18]. No charging occurred during the first half of this eclipse and the frame potential was greater than -1 kV during the second half.

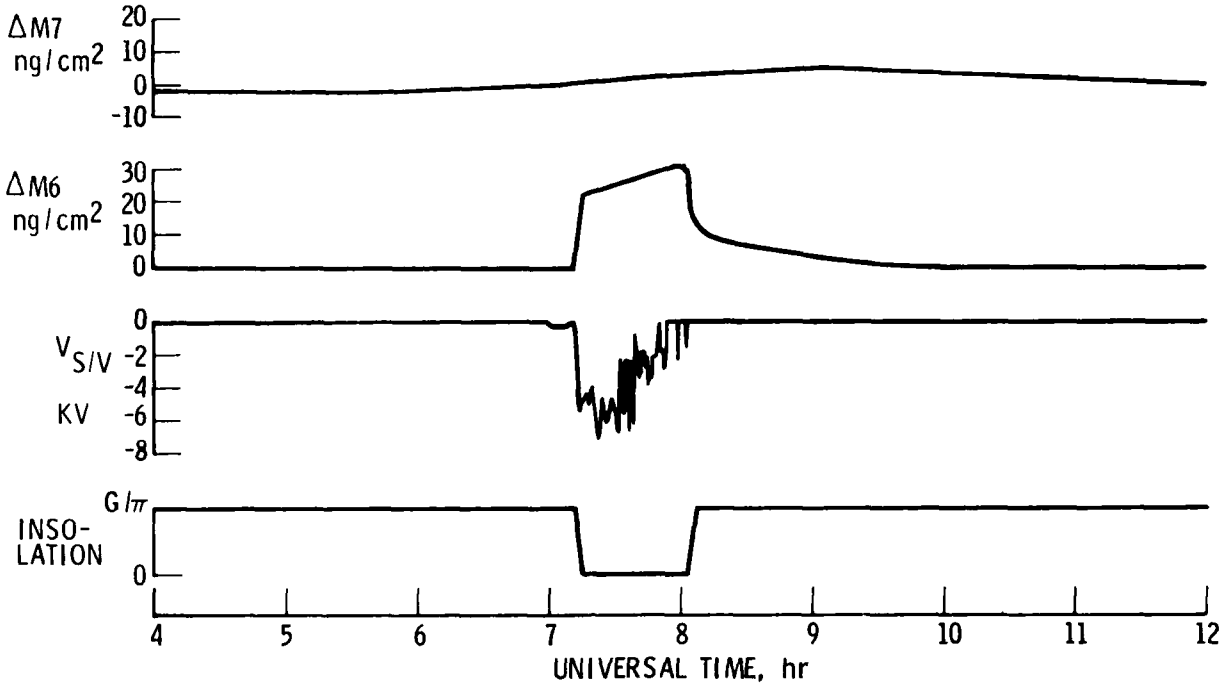

Fig. 17. ML-12 Mass Accumulation During Large P78-2 Charging in Eclipse on Day 114, 24 April 1979

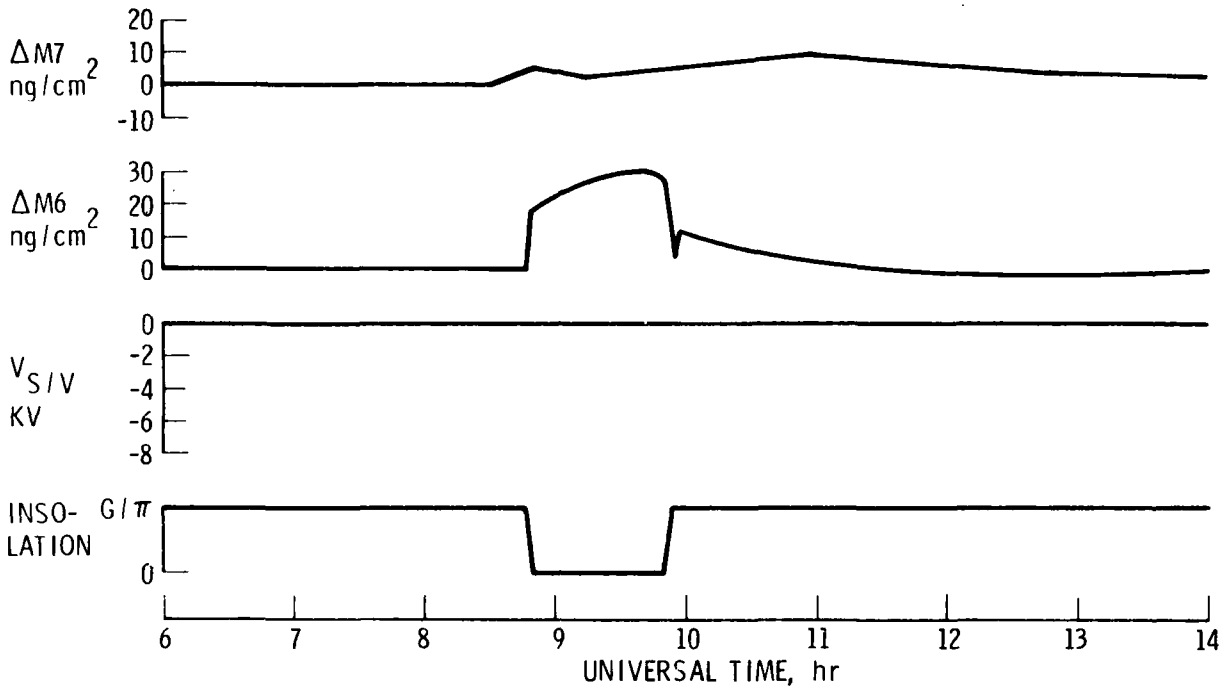

Fig. 18. ML-12 Mass Accumulation During Quiet P78-2 Eclipse on Day 109, 19 April 1979.

As in the case of M7, the M6 response is very likely due to thermal effects. The rapid increase in indicated mass value which occurs during the first two minutes or so of the eclipse is entirely consistent with the instrument response repeated every spin period in sunlight. As the sun passes out of the field of view, the radial thermal gradient it induces in the quartz crystal rapidly dissipates and the resonant frequency shifts. (In the M6 data plots, this sizable oscillation in apparent mass has been omitted for clarity; the data used is that obtained from the sensor just before the sun enters the field of view.)

The data of the Day 114 eclipse is interpreted to indicate that the accumulation rate of electrostatically reattracted molecules was less than the experimental resolution under those conditions: approximately 1 ng/cm^2 hr. Caufman [Ref. 8] estimates the electrostatic recapture coefficient to be of the order of 5×10^{-4}. When this value is used together with estimates of the P78-2 outgassing rate of condensables, return fluxes predicted are also less than 1 ng/cm^2-hr. . .

The next paper covering the ML12 RPA/TQCM results, Ref. 35, was also solicited by the session chairman. It was prepared in December of 1979. By then the major differences between the data from the shadowed and sunlit TQCMs were apparent and photolysis was strongly suspected as the reason:

The mass accumulation rate on the ML12-7 TQCM has exhibited a definite dependence on sensor temperature. This dependence is shown in [Table 6], which provides mass accumulation rates for orbital periods when sufficient data were analyzed to yield unambiguous rates. During those periods when the temperature of the ML12-7 mass detector exceeded -30°C, the detector lost mass (negative mass accumulation rate); when the temperature of the detector was at -30°C and below, it gained mass. Accumulation rates are considerably greater in the -90 to -100° range, which occurs when no heater power is used. The rates given in the table are equilibrium values; transient responses to temperature commands have not yet been analyzed.

In contrast, the ML12-6 TQCM mass accumulation rate is relatively insensitive to detector temperature. During the first months on orbit, this sensor cooled to -40°C when the heater was turned off and the spacecraft was in sunlight. (The ML12-6 and -7 are nominally identical pieces of hardware, but an average of 431 W/cm^2 of sunlight is incident on the ML12-6 radiator, whereas the ML12-7 is continuously shadowed. More recently, the average temperature of the ML12-6 detector in sunlight with no heater power has been about -34°C.) As is shown in [Table 6], the mass accumulation rate on ML12-6 has been consistently larger than on ML12-7 and remains positive even at 58°C.

Table 6. Equilibrium Mass Accumulation Rates of ML12-6 and ML12-7 During Several Orbital Periods in 1979

	ML12-7		ML12-6	
Period (Julian Day)	Detector Temperature (°C)	Equilibrium Mass Accumulation Rate, ML12-7 (ng/cm^2-day)	Detector Temperature (°C) (Corrected)	Equilibrium Mass Accumulation Rate, ML12-6 (ng/cm^2-day)
44-66	-90 to -100	2.6	-38 to -41	18.6
66-88	-90 to -100	5.6 to 11.5	-38 to -63	15
93-117	-30	0.6	-38	11.2
119-130	0	-1.9	-7	9.8
131-172	20 to 25	-0.5	24 to 58	8.1
187-199	-30	0.8		
243-268	-90 to -103	2.1	-38	4.7
268-308	-30	0.2	-35 to -39	4.7
308-332	-91 to -100	2.1	-34 to -37	5.8

The general shape of the ML12-6 mass accumulation versus time curve is similar to that of the function

$$M6 = K_1(1 - e^{-K_2 t})$$

where K_1 and K_2 are constants. This function is also the time dependence of mass accumulation observed in the laboratory when a cold QCM is exposed in vacuum to a warm organic material outgassing a single molecular species. Since the most abundant sources of molecules from P78-2 are probably organics that are outgassing, the observed shape of the accumulation rate versus time curve is expected. However, in laboratory experiments, the accumulation rate decreases as the QCM temperature is increased above some temperature because re-evaporation from the detector becomes significant. Because of the insensitivity of the ML12-6 mass accumulation rate to its sensor temperature, it appears that either the material being collected initially has a high desorption energy (i.e., a high temperature is required to cause it to evaporate), or that ultraviolet (uv) is increasing the desorption energy of the material. The first hypothesis requires that the material be outgassed from a solid that is warmer than the detector or be released through some process other than evaporation. It is not likely that any part of P78-2 exceeds 58°C. At present, the effect of uv on either the arriving molecules or the surface to which they absorb (the second hypothesis) is considered the most likely explanation of the insensitivity of ML12-6 mass accumulation rate to detector temperature...

A statistical approach was adopted in the search for evidence of contamination rate enhancement by spacecraft charging. The effect of retarding potential grid voltage (RPAV) on mass accumulation rate was averaged over long periods of time, rather than being observed only during periods of known spacecraft charging. This approach was necessary because major natural P78-2 charging events of significant duration seemed to be restricted to eclipses. As mentioned earlier, eclipse thermal effects in the instruments raised their detection limits. Also, photoionization, the main mechanism of molecular ionization, is absent during eclipses. The paper of Ref. 42 was presented to the spacecraft charging community in November 1980 detailing the results of the first two statistical experiments conducted:

In this paper are reported two experiments that deal with these difficulties statistically. The assumptions made are: (1) charging events are approximately uniformly distributed in time, (2) charging events are large enough, long enough, and frequent enough to make $\dot{M}^+/\dot{M}^o$ detectable, (3) the rate and composition of mass release from the vehicle are approximately constant over an experimental period, and (4) the adsorption

characteristics of mass incident on the mass detector are constant with time. In both experiments, the aperture grid was connected to the spacecraft frame. The coating over the mirrors surrounding the aperture and the skin of the spacecraft out to 25 cm from the aperture are electrically conductive and are also connected to the space vehicle frame. Therefore the electric field in the vicinity of the aperture must be relatively uniform and perpendicular to the aperture plane. The RPA grid voltage was commanded to selected values for periods of 10 or more days, and $\dot{M}$ values averaged over 5-day segments were compared.

In the first (winter) experiment, a greater than 90 percent confidence was obtained that $\dot{M}$ is negatively correlated with RPAV, i.e., that some incoming mass is reflected by the grid when it is positively biased. This fraction of the mass must have been positively ionized. The outcome of the recently concluded second (summer) experiment is not as easily assessed. The validity of data from three of the eight experiment segments is questionable and not as yet resolved. Some evidence of negative correlation is obtained when these data points are included in experiment analysis. If the questionable data points are excluded from the summer analysis, however, there is strong evidence of the negative correlation of $\dot{M}$ with RPAV. . .

The results of the RPA winter and summer experiments are tabulated in [Table 7] and plotted in [Figures 19 and 20]. Each value of $\dot{M}_6$ reported represents the average mass accumulation rate over a 5-day period, and the error bars shown are $\pm S_1'$. In both experiments, the mass accumulation rate was smaller when RPAV was 500 V than for other values. This is consistent with the idea that reattracted positively ionized contaminants are reflected by the grid. Less easily understood are the values of $\dot{M}_6$ when RPAV was 100 V, because theory predicts $\dot{M}_6$ (100) $\leq \dot{M}_6$ (RPAV $<$ 100). One explanation is that vehicle charging might have been more prevalent than normal during these high $\dot{M}_6$ periods. It is anticipated that the eventual availability of all agency tapes for the experiment periods will provide further clues to this feature of the data.

To determine the extent to which the $\dot{M}$ values were correlated with RPAV, linear regressions of $\dot{M}6$ versus RPAV were calculated separately with data from the winter and summer experiments. In this analysis, a single linear function was fitted to all data from each experiment. . . Theory results in the expectation of a more complicated functional dependence of $\dot{M}$ on RPAV. However, the size of the data set in this case did not justify fitting a more complex curve to the data. The correlation coefficients associated with these linear regressions of $\dot{M}_6$ versus RPAV were also calculated. If the data are assumed to be normally distributed, levels of confidence can be assigned to the validity of the hypothesis that $\dot{M}_6$ is negatively correlated with RPAV, i.e., that contamination is enhanced by spacecraft charging. The results of these analyses are summarized in [Table 8].

Table 7. ML12-6 TQCM Mass Accumulation Rates at Various RPA Bias Settings (Grounded Aperture Grid Condition)

Grid Bias Level (Volts)	Accumulation Rate (ng/cm^2-day)	Statistical Standard Error (ng/cm^2-day)
	Winter Experiment	
+500	5.662	±0.265
-100	7.483	0.270
-10	6.761	0.308
+10	7.018	0.360
+100	8.069	0.337
	Summer Experiment	
-100	1.994	0.288
-100	2.088	0.346
+100	1.044	0.317
+100	3.550	0.314
+100	1.886	0.310
+500	2.172	0.327
-100	3.101	0.311
-100	3.000	0.345

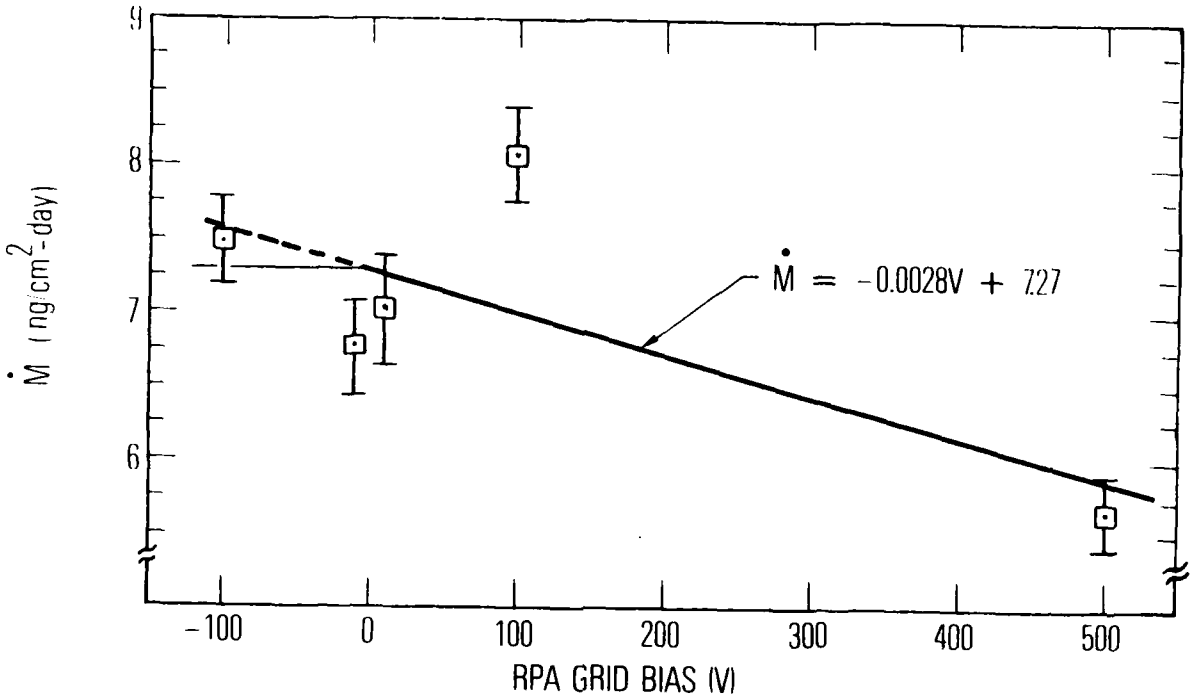

Fig. 19. ML12-6 TQCM Mass Accumulation Rates at Various RPA Grid Bias Potentials During Winter Experiment

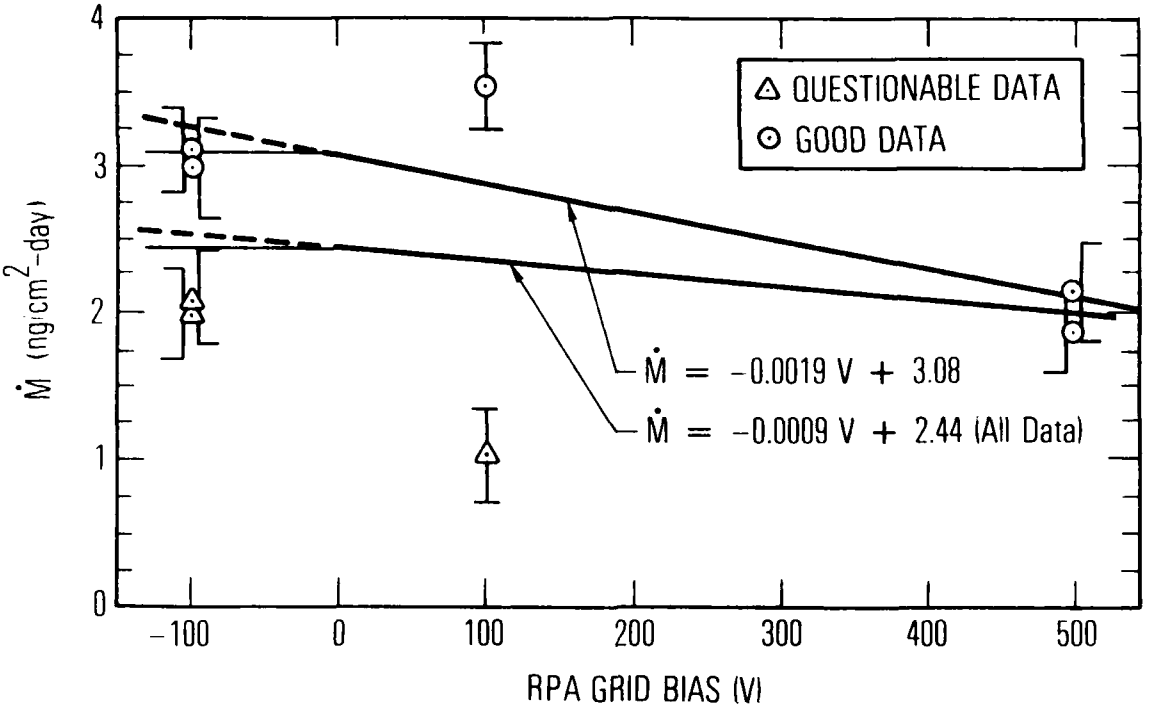

Fig. 20. ML12-6 TQCM Mass Accumulation Rates at Various RPA Grid Bias Potentials During Summer Experiment

Table 8. Correlation of ML12-6 TQCM Mass Accumulation Rates with RPA Bias Levels (Ground Grid Configuration, 100 V ≤ RPAV ≤ 500 V)

Experiment Segment	Regression Coefficient $(ng/cm^2\text{-day})/volt$	Correlation Coefficient (r)	Level of Confidence that $r < 0$	Average Ionized Mass (KE < 500 eV)
Winter	-0.0028	-0.721	~ 91%	19%
Summer (Abbreviated)	-0.0019	-0.828	~ 98 %	31%
Summer (All Data)	-0.0009	-0.279	~ 75 %	18%

The winter experiment results provide a level of confidence of approximately 91 percent in the negative correlation of $\dot{M}_6$ with RPAV. The sensitivity of $\dot{M}_6$ to RPAV for the winter experiment is calculated to be

$$\frac{d\dot{M}_6}{dV} = \frac{-0.0028 \text{ ng/cm}^2\text{-day}}{\text{volt}}$$

between limits of $-100 \text{ V} \leq \text{RPAV} \leq 500 \text{ V}$.

The results from the recently concluded summer experiment are complicated by the fact that data points from three of the eight experiment segments are somewhat questionable, but no unimpeachable grounds were found for excluding them. These are the two smaller $\dot{M}_6(-100)$ values and the smaller $\dot{M}_6(100)$ value plotted in [Figure 20] with triangular symbols. The $\dot{M}_6(100)$ value is questionable because the $\dot{M}_6$ versus time data from which it was derived could be better characterized by a "sawtooth" waveform than by a "ramp." Although $\dot{M}_6$ for the experiment segment as a whole is unusually low, values of $\dot{M}_6$ for the two individual sawtooth "teeth" in the segment closely approximate other summer values. One of the $\dot{M}_6(-100)$ values represents a period in which the data set is very small because of a temporary reduction in the number of data transmissions per day. The remaining $\dot{M}_6(-100)$ value is from the first summer experiment segment, which began 2 days after a TQCM temperature command was issued. Although thermal equilibration time required after such commands is usually only 1 day, it is variable and could influence the data set. Final resolution of TQCM behavior during these three periods will not be possible until appropriate agency tapes are examined.

If the questionable data points are excluded from analysis, the results of the summer experiment provide a 96 percent level of confidence in the negative correlation of $\dot{M}_6$ with RPAV. The sensitivity in this case is calculated to be

$$\frac{d\dot{M}_6}{dV} = \frac{-0.0019 \text{ ng/cm}^2\text{-day}}{\text{volt}}$$

between limits of $-100 \text{ V} \leq \text{RPAV} \leq 500 \text{ V}$. If the questionable data points are included in the analysis, the sensitivity of $\dot{M}_6$ to RPAV for the summer is calculated to be

$$\frac{d\dot{M}_6}{dV} = \frac{-0.0009 \text{ ng/cm}^2\text{-day}}{\text{volt}}$$

and a 75 percent level of confidence in the negative correlation of $\dot{M}_6$ with RPAV is obtained.

These linear regressions, which have the form

$$\dot{M}_6(\text{RPAV}) = \dot{M}_6(0) + \text{RPAV}\,\frac{d\dot{M}_6}{dV}$$

were used to estimate the average percentage of the mass arriving at the detector that was ionized and had kinetic energy of less than 500 eV. This percentage is given by

$$\frac{\dot{M}^+}{\dot{M}^o + \dot{M}^+} = \frac{-500\ d\dot{M}_6/dV}{\dot{M}_6(0)} \times 100$$

and the value ranges from 18 to 31 percent as shown in [Table 8].

As noted in the discussion of extraneous effects, variations in solar irradiance appear to affect the rate of mass accumulation. Data obtained during the RPA experiment support the observation that the presence of sunlight enhances the accumulation of mass on surface. Specifically, values of $\dot{M}_6$ during periods of [partial] shadowing [of the detector lay booms] are as much as 30 percent lower than those observed during non-shadowed periods. . . In addition, values of $\dot{M}_6$ for periods of lesser average solar irradiance near perihelion are as much as 45 percent lower than those observed during periods near aphelion. During both the winter and summer experiments, accumulation rates for the shadowed ML12-7 TQCM have seldom exceeded 1 ng/cm^2-day, whereas, the insolated ML12-6 TQCM rates have ranged from approximately 2 to 8 ng/cm^2-day. It is suspected that this phenomenon is the result of photochemical reactions at or near the adsorbing surface.

The next two papers reported our search for evidence of contamination associated with firing of thrusters on board P78-2. The ML12 payload was not designed to optimize the measurement of thruster related contamination, and no contamination increase was detected at thruster firing times. However, these analyses establish upper bounds on molecular film contamination depositing at the ML12 sensor locations.

In Ref. 23 ML12 data collected at the time of the solid propellant kick motor firing were examined:

The solid propellant apogee insertion motor (AIM) on board the P78-2 satellite was manufactured by United Technology and uses approximately 550 lb of Al/NH_4ClO_4 propellant. It is of the same general design as that of the inertial upper stage (IUS) that will raise payloads from space shuttle orbits to higher altitudes. However, the AIM motor had a polybutadiene acrilonitrile (PBAN) propellant binder whereas the newer hydroxy terminated polybutadiene (HTPB) binder is used in the IUS. . . Contamination effects arising from the firing of the AIM would be of interest to the IUS users and manufacturer.

Several of the contamination detectors on the P78-2 satellite were operating prior to, during, and following the AIM burn. . . These sensors are capable of detecting condensable materials and/or ions. They are not very effective at monitoring particulates, which are another class of contaminants produced by solid propellant rockets. The location of detectors active at the time of the AIM burn is shown in [Figure 2]. (It was not possible to open the cover of the TQCM located between the TCC trays before the AIM firing because the vehicle was then spinning at 60 rpm.) These locations were not chosen as ideal AIM exhaust product detection sites since that was not the primary goal of the ML12 experiment. Nevertheless, the data from these sensors have been analyzed to look for contamination due to the firing of AIM. . .

A listing of various TCCs being monitored on the ML12 package is presented in [Table 9]. Also listed are the on-orbit temperatures of these materials, the inherent uncertainty of the circuitry for determining their solar absorptances, and the change in the solar absorptances as measured before and after the AIM burn. On all these materials it can be noted that the changes in the solar absorptances are comparable to, or substantially less than, the uncertainties of the measurements. Of these samples, the uncoated optical solar reflector (OSR) is the best test for contamination. It is among the most space stable of the TCCs; therefore, degradation unrelated to contamination is minimal. Also, its optical properties cause it to have the lowest on-orbit temperature, making it the best trap for condensable materials.

At the time of the AIM burn, the TQCM temperature was 30°C. The RPA was set at 0 V with respect to the vehicle frame, and the aperture grid was also grounded to the frame.

The resolution of the TQCM circuitry coupled with the partial shading by the RPA grids means that a minimum mass deposition of 2.4 ng/cm^2 can be detected. No evidence of this magnitude of mass deposition was observed, however.

Finally, the RPA is the most sensitive of the ML12 instruments for monitoring the influx of contaminants, if they carry a charge. The data from this sensor, for a period prior to and 2 hr after the AIM burn, are presented in [Figure 21]. The AIM burn commenced at 21.73 hr universal time and lasted ~30 sec [shown in Figures 21a and 21b]. During that time

Table 9. P78-2 AIM Burn Contamination Effects on TCCs

Sample	Temperature, °C	$\Delta\alpha_s$	Approximate Uncertainty, $\Delta\alpha_s$
OSR (mirror)	-42	-0.003	±0.01
In_2O_3/OSR	-41	-0.011	±0.014
2 mil Teflon FEP	-37	-0.002	±0.009
5 mil Teflon FEP	-38	-0.001	±0.009
Fabric/FEP/Al	-32	+0.006	±0.008
Polished Al	36	-0.013	±0.009
Polished Al	35	-0.001	±0.009
Fabric/Tape	-28	+0.002	±0.012
Au	46	-0.006	±0.01
Conductive Paint	-28	+0.004	±0.01
Thin Au/Kapton/Al	19	+0.006	±0.011
Kapton/Al	-11	-0.003	±0.01
Grafoil	39	+0.001	±0.013

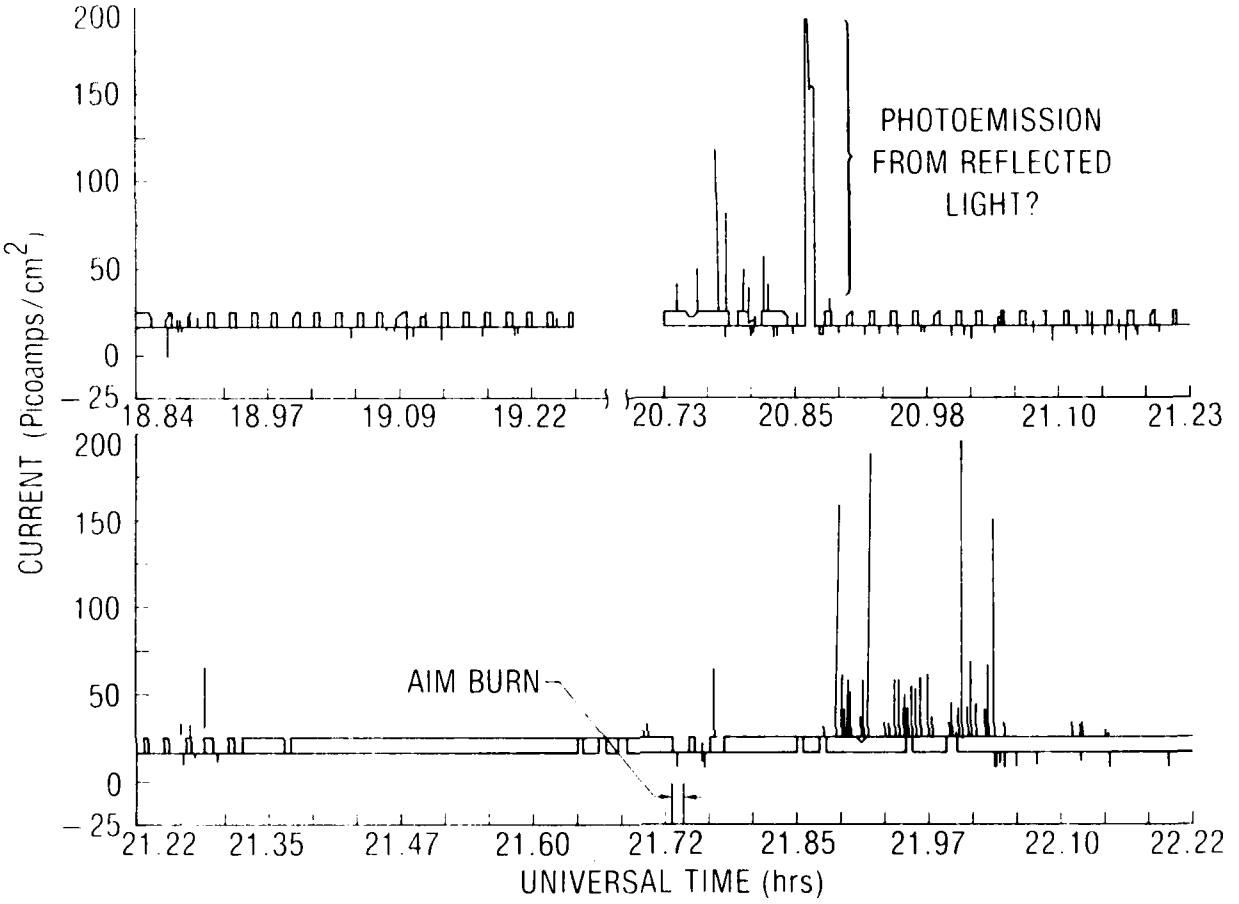

Fig. 21a. RPA Electrometer Current Density Vs. Time in the Period Preceding and Immediately Following the AIM Burn at 21.73 Hr

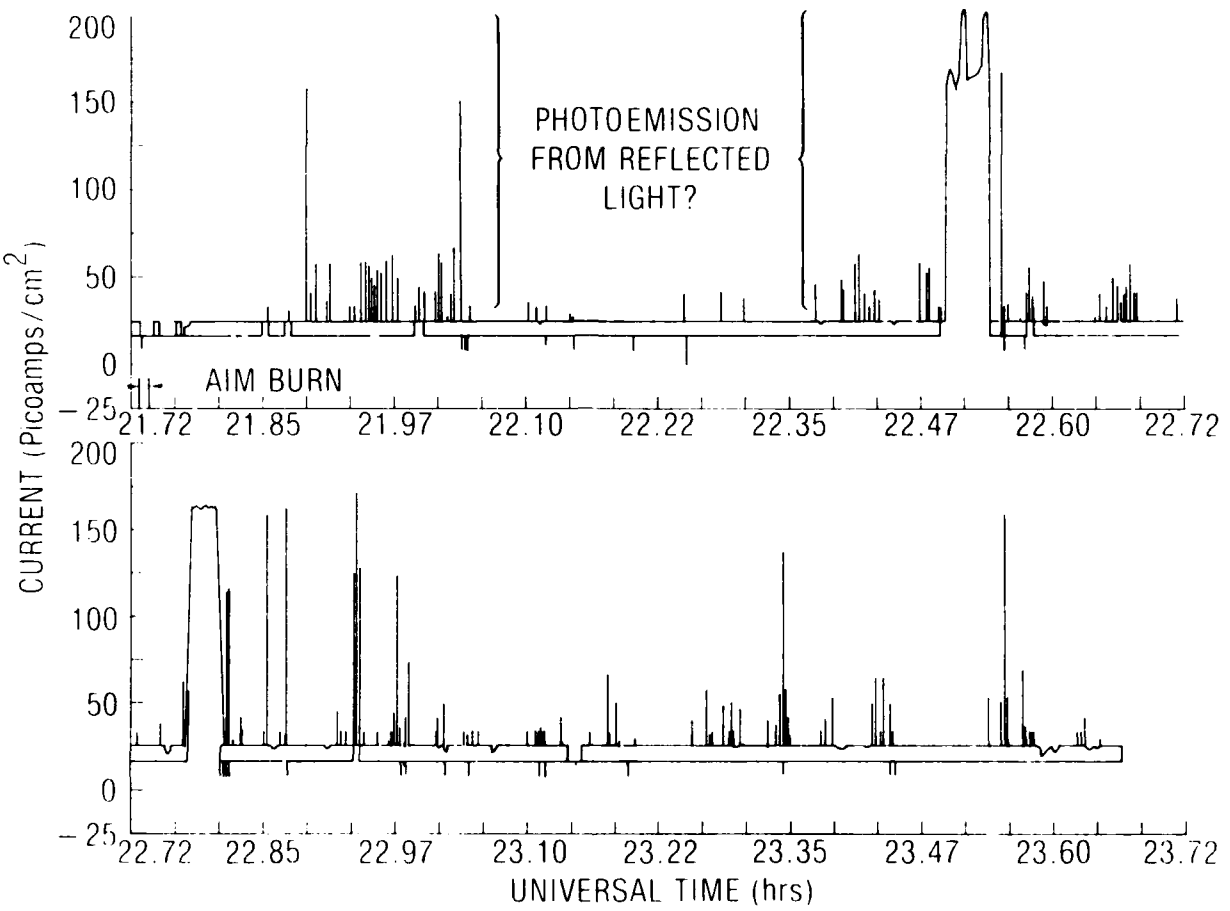

Fig. 21b. RPA Electrometer Current Density Vs. Time in the 2-Hr Period Commencing with the AIM Burn

the RPA grid voltage was 0 V. It is seen in [Figure 21] that there was a positive background current of 15 to 25 pA/cm^2 during the entire period (and, in fact, during all data periods up to a maneuver 28 hr later when the vehicle attitude was changed such that ML12-7 was no longer illuminated). This current is primarily due to photoelectron emission from the charged particle collector rather than from positive ion influx. Such photoemission was observed during the preflight calibration of the RPAs.

In addition to the background current, there are also positive current "spikes" present in the data of [Figure 21]. These spikes range between 1 and 200 sec in duration. One speculation is that they are ionized contaminants released during the AIM burn and constrained to helical paths by the ambient magnetic field of the Earth. However, it is felt that a more likely explanation is that they are photoemission currents caused by light reflected from the part of the spacecraft communication antenna that is within the ML12-7 field of view. Indeed, at least one long (~25 sec) and 16 short spikes occurred before the AIM burn [Figure 21a]. In this hypothesis, the lack of simple periodicity of these spikes is explained by spacecraft nutations causing the reflections to partly or completely miss ML12-7 most of the time.

Disregarding the photoemission hypothesis and assuming the spikes to be caused by charged contaminants, the total charge collected during the 2 hr comes to 5×10^{11} electronic charge/cm^2. If a large very atomic mass unit/electronic charge ratio of 1000 is used for the supposed contaminants, this influx amounts to only approximately 0.8 ng/cm^2. Were an influx of this magnitude to form a uniform unity density thin film, its thickness would be ~ 0.08 Å. Thus, at least at the location of ML12-7, the upper bound on charged contaminants collected during the 2 hr following the AIM burn was insignificantly small.

[To summarize] measurable contamination was not recorded by the ML12 sensors operational at the time of the AIM burn. The detection threshold of the TCC calorimeters, which are located ~ 0.9 m behind the nozzle and view perpendicularly to the thrust vector, was $\Delta\alpha_s = 0.001$. The threshold of the 30°C TQCM, which was located ~1.75 m behind the nozzle and viewed 180 deg from the thruster plume, was ~2.4 ng/cm^2. The RPA, which is integral to the TQCM, could have measured currents of ionized contaminants greater than ~10 pA/cm^2.

Obviously, the location of the active RPA/TQCM with respect to the thrust plume minimized the possibility of collecting thruster contaminants. This location was selected to serve experimental goals unrelated to thruster contamination. Also, the TQCM sensing surface was aluminum and connected to spacecraft ground, so particulates, if present, would not have adhered well to this vibrating surface. When TQCMs are intended for the measurement of particulates, an adhesive coating is frequently employed.

The locations of the trays of TCC calorimeters were more favorable for the detection of contamination from the thruster though probably not optimum. As with the TQCM, the TCC calorimeters are most sensitive to molecular contamination. In particular, the calorimeters are not sensitive to changes in the specular reflectance of polished metal samples. Therefore, it is conceivable that a high quality sensor mirror in this location might have detected contamination even though the calorimeters did not.

Finally, the P78-2 probably was not charged significantly by the ambient space plasma at the time the AIM was fired. (Since the other instruments on the vehicle were not operating during this period, the vehicle potential cannot be determined, but significant charging would have been noticed indirectly in the magnitude of the RPA current.) Had the plasma charged the vehicle and maintained the charge during the firing, at least some ionized thruster products would have been electrostatically reattracted to the vehicle. However, during charging events the density of energetic electron currents rarely exceeds 1×10^{9} A/cm^{2}. For the vehicle to have remained negatively charged, any influx current of positive ion contaminants could not have exceeded this electron current. Taking 1×10^{9} A/cm^{2} as a limiting value for such an ion current, one still obtains a very low total influx of charge in the ~30-sec burn period.

The analysis of ML12 data obtained at the time of a number of hydrazine thruster firings is presented in Ref. 22. Several of the maneuvers studied altered either the angle the sun line formed with the spin axis or the rate of vehicle rotation. Since both of these types of change affect the exposure of ML12-6 to sunlight, it was necessary to perform a much more sophisticated analysis of the ML12-6 data than the usual comparison of peak readings. The following excerpts describe the thruster locations and the results of the analysis:

The SCATHA satellite reaction control system consists of two rocket engine modules (REMs) located on the bottom of the cylindrical satellite structure. Each REM has four rocket motors: two 0.23-lb$_f$ spin engines, one 0.23-lb$_f$ precession engine designated as a low thrust engine (LTE), and one 6.5-lb$_f$ precession engine designated as a high thrust engine (HTE). The location of the REMs with respect to the satellite and the ML12 payload is shown in [Figure 22].

The spinup and spindown maneuvers required constant thruster operation, whereas in the LTE and HTE maneuvers, pulsed thruster operation was used. The hydrazine propellant conformed to MIL-P-2653C. . . Detailed analysis of the P78-2 engine performance is available in [Ref. 21].

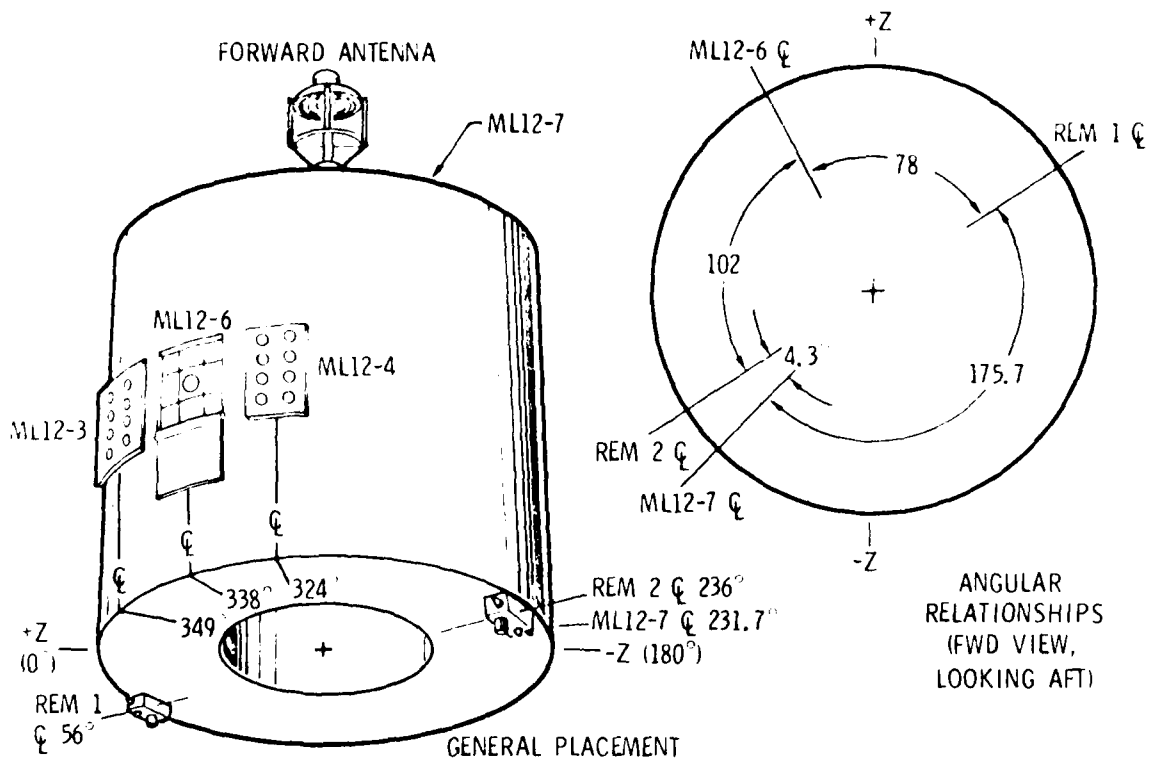

Fig. 22. Locations of ML12 TQCM/RPA Sensors and Hydrazine Rocket Engine Modules on the P78-2 Satellite. The satellite is approximately 1.75 m in length and 1.75 m in diameter.

The satellite maneuvers involving the hydrazine thrusters are of three distinct types: major precessions of the satellite spin axis using the large thrusters (HTE), spinup and spindown maneuvers, and minor precessions using the small thrusters (LTE). The specific maneuvers chosen for analysis were those that would offer the best opportunity to detect thruster-related contamination. One HTE precession, one despin, and ten LTE precession maneuvers were analyzed. Although it was not chronologically the first of the selected maneuvers, the results of the analysis of the despin maneuver are required for the analysis of the HTE precession maneuver. Therefore, the despin maneuver is discussed first. The LTE precession maneuvers are discussed last.

The SCATHA spin rate was reduced from 62.1 to 1.047 rpm after the spacecraft was inserted into final orbit by means of a series of maneuvers involving the spinup-spindown motors. The maneuver that reduced the spin rate from 15 to 1.5 rpm was chosen for analysis for two reasons: (1) the ML12-6 sensor cover was closed during launch and was not opened until the spin rate was 15 rpm, and (2) the maneuver was long, lasting 260 sec with the thrusters firing constantly. . .

. . .no mass collected as a result of the despin maneuver within the ± 6 ng/cm^2 accuracy of the method. . .

. . .neither the mass nor current detectors located on the equatorial band of the vehicle show evidence of contamination from the spin-down thrusters.

No change in current or mass values as a result of the spin-down maneuver is evident in the data from ML12-7 (not shown). Since the instrument was shadowed at the time, neither signal was modulated by sunlight effects.

The large precession motors were fired several times during the early stages of the mission to orient the spacecraft for upcoming maneuvers. The HTE precession maneuver that was selected for analysis occurred with the spacecraft rotational rate at 15 rpm, two days after the opening of the ML12-6 cover. Each engine was fired for 215 pulses, resulting in the spacecraft spin axis rotating from 46 to 97 deg relative to the spacecraft-sun line. . .

Thus, no contamination was detected by the ML12-6 TQCM. The ML12-6 RPA data (not shown) support this conclusion in that there are no major current artifacts associated with the precession maneuver. There are some small current effects, probably caused by photoemission from the RPA collector, that begin approximately two-thirds through the maneuver and continue for some time after. The amplitudes of these effects were so small that they were not significant even if caused by contamination rather than photoemission.

The ML12-7 mass, temperature, and current data (not shown) for the precession maneuver also were analyzed. No effects were detected that could be attributed to sensor contamination.

During operation in final orbit, the satellite spin axis precesses approximately 1 deg/day. To compensate for this motion, the 0.23-lb_f LTE precession motors were fired once per week to maintain the spacecraft spin axis at 90 ± 5 deg with respect to the spacecraft-sun line. This spacecraft orientation places the ML12-6 sensor in the sun once per spacecraft revolution but keeps the ML12-7 sensor always in the spacecraft shadow.

For the period 17 March through 22 December 1979, ten LTE precession maneuvers were analyzed. The individual maneuvers were selected to give a large number of pulses and to represent various TQCM temperatures and RPA states. . .

The maximum mass values exhibit no [ML12-6] mass increases during the firing of the thrusters. . .

No thruster-related changes were observed in the ML12-7 mass and ML12-6 and ML12-7 charged particle detector data sets. Thus, it can be concluded that no mass or current increases resulted from the ten selected precession maneuvers in which the axial LTEs were used.

The most recent publication containing results from the RPA/TQCM instruments is Ref. 43:

. . . In this paper are given long-term mass-accumulation data from the mass detector mounted on the equatorial band of the vehicle, and long-term α_s data from the four space-stable TCC samples. The TCC samples are in trays located a few inches from either side of the mass detector. The data indicate that non-line-of-sight (non-LOS) contamination-transport mechanisms are at work at synchronous altitude, and that most of the "space-stable" TCC samples have increased α_s since launch. These increases are thought to be caused by contamination. The increase in α_s of a fused-quartz mirror is related to the quantity of mass collected on the nearby TQCM.

[Figure 23] is a top view of the P78-2 vehicle with booms deployed. Note that the RPA/TQCM (ML12-6) has no objects in its 130-deg field of view (FOV), and that the TCC samples (ML12-3 and -4) have only a negligible view factor with the SC2-1 and SC11 booms. Therefore, to a good approximation these detectors have a free FOV, and contamination molecules reaching them must do so by other than LOS trajectories. Nevertheless, the flight data indicate that many molecules have reached the detectors and adsorbed on them.

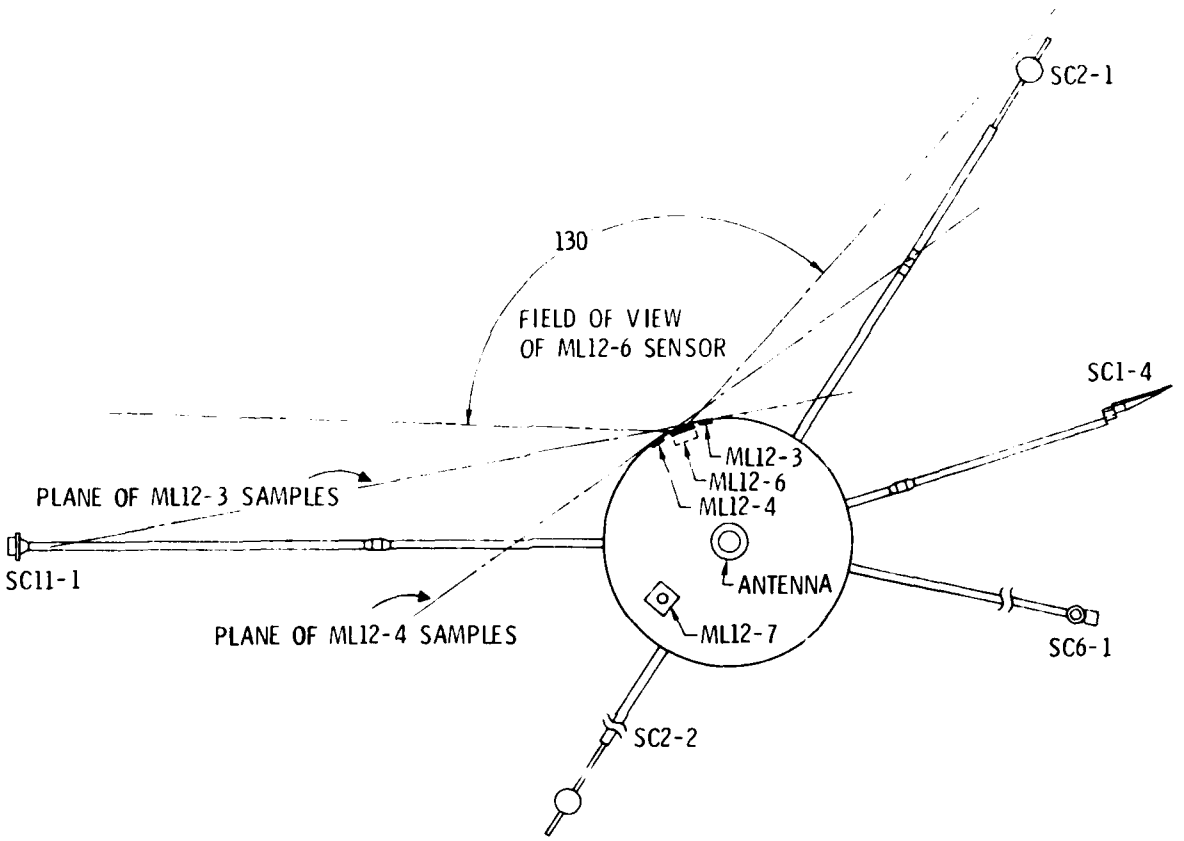

Fig. 23. Scale Drawing of P78-2 Viewed Along Vehicle Spin Axis Showing that ML12-3, -4, and -6 Sensors Have Nearly Free Fields of View

[Figure 24] is a plot of the amount of contamination collected on the MI.12-6 TQCM as a function of time from launch. In [Figure 24] the scale of the ordinates has been corrected for the optical density of the RPA grids in front of the sensor crystal and converted to thickness units under the assumption that deposits are of uniform thickness and unity density (1 g/cm^3). The sudden changes in indicated thickness are primarily the result of TQCM frequency shifts resulting from commanded changes in detector temperature. These shifts will eventually be edited out of the data, because they are artifacts of the instrument. . .

If the increase in α_s of the nearby fused quartz mirror is ascribed to contamination, and if it is assumed that the thickness of the contamination is the same on the mirror and the TQCM, it is then possible to plot the increase in α_s as a function of thickness. As shown in Fig. 25, this functional dependence is linear over the first 500 Å with

$$\frac{d\alpha_s}{dx} \simeq 1.3 \times 10^{-5} \text{Å}^{-1}$$

This value is in reasonable agreement with a calculation due to Zeiner,[44] the results of which are also shown in Fig. 25. Zeiner's calculation is based on the solution of Maxwell's equations for propagation of a plane electromagnetic wave through a thin, coherent film on top of a thick, incoherent fused-silica silvered mirror. Reflections are computed at all interfaces. The solar absorptance is computed from a solar-spectrum-weighted average of the computed spectral absorptances over the range of 0.2 to 6 μm. The optical absorption of the thin film was taken as an average of the data in Fig. 26. These data are probably uncertain by at least 50%.

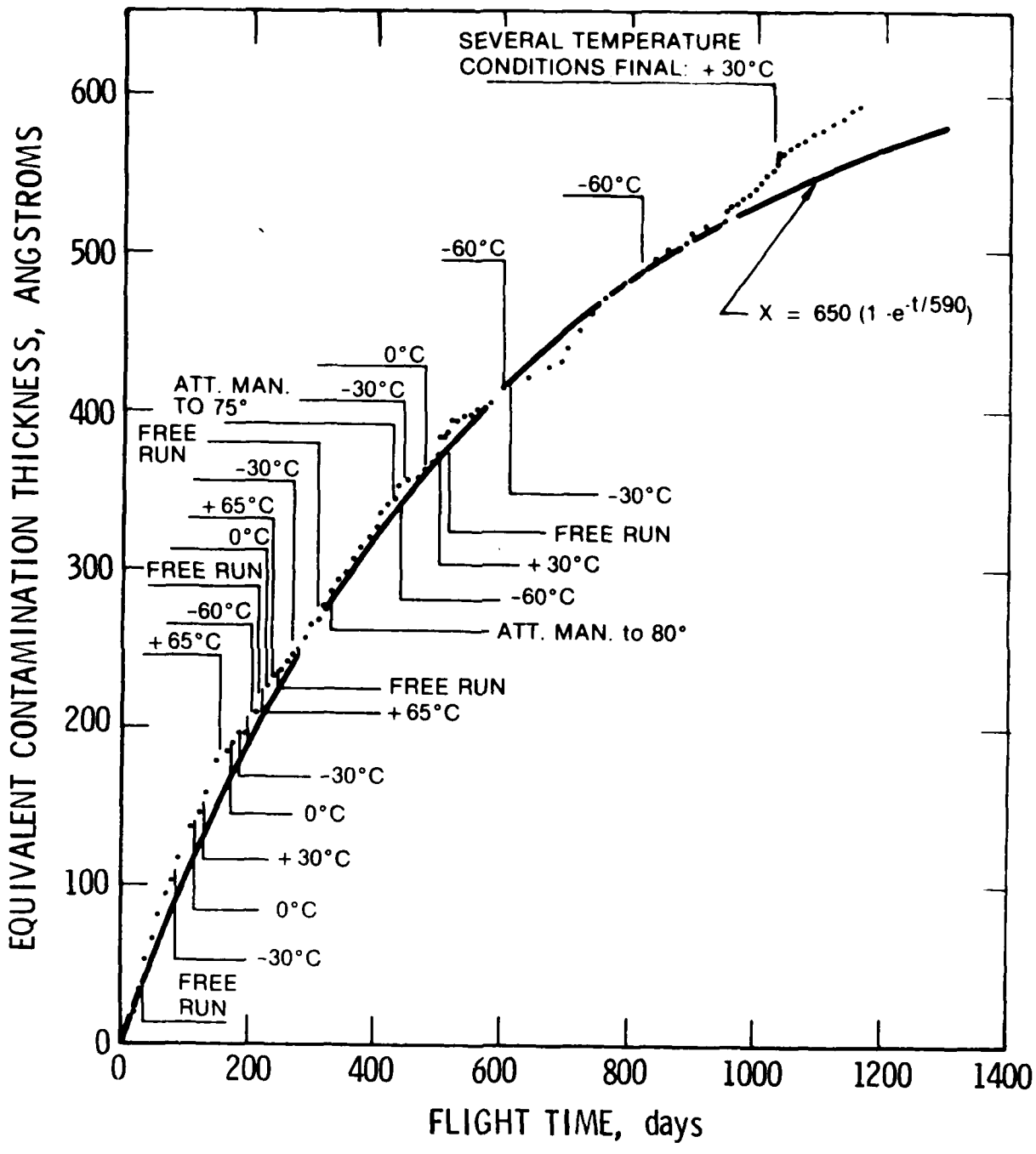

Fig. 24. Thickness of Contamination Collected on ML12-6 Temperature-Controlled Quartz-Crystal Microbalance, Assuming It Is a Uniform, Unity-Density Film. Sensor-temperature commands and curve fit are also shown.

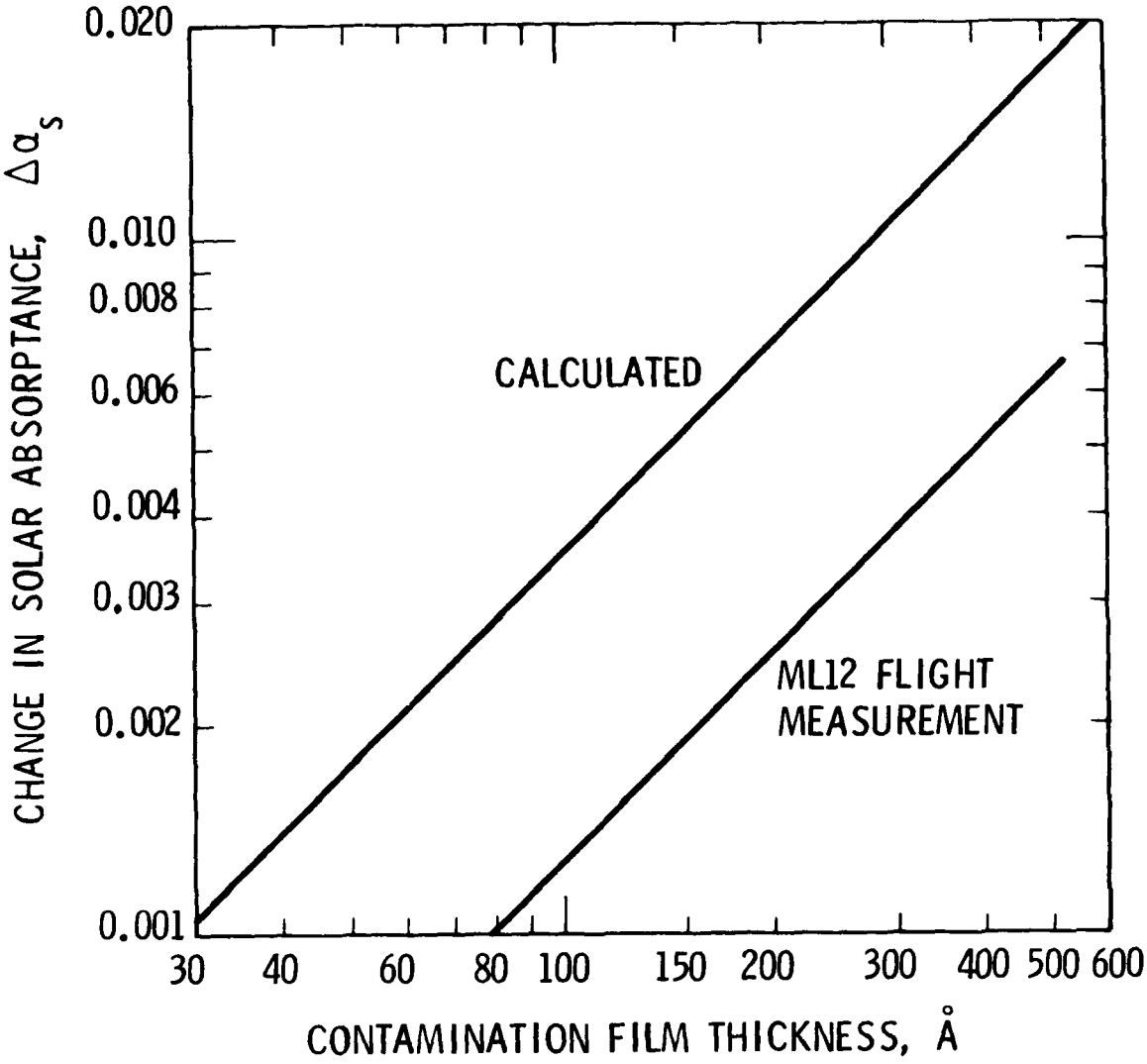

Fig. 25. Plot of Change in Solar Absorptance of Fused-Quartz Mirror (OSR) Vs. Thickness of Unity-Density Contamination Film, According to Theory (Ref. 44) and ML12 Flight Measurements

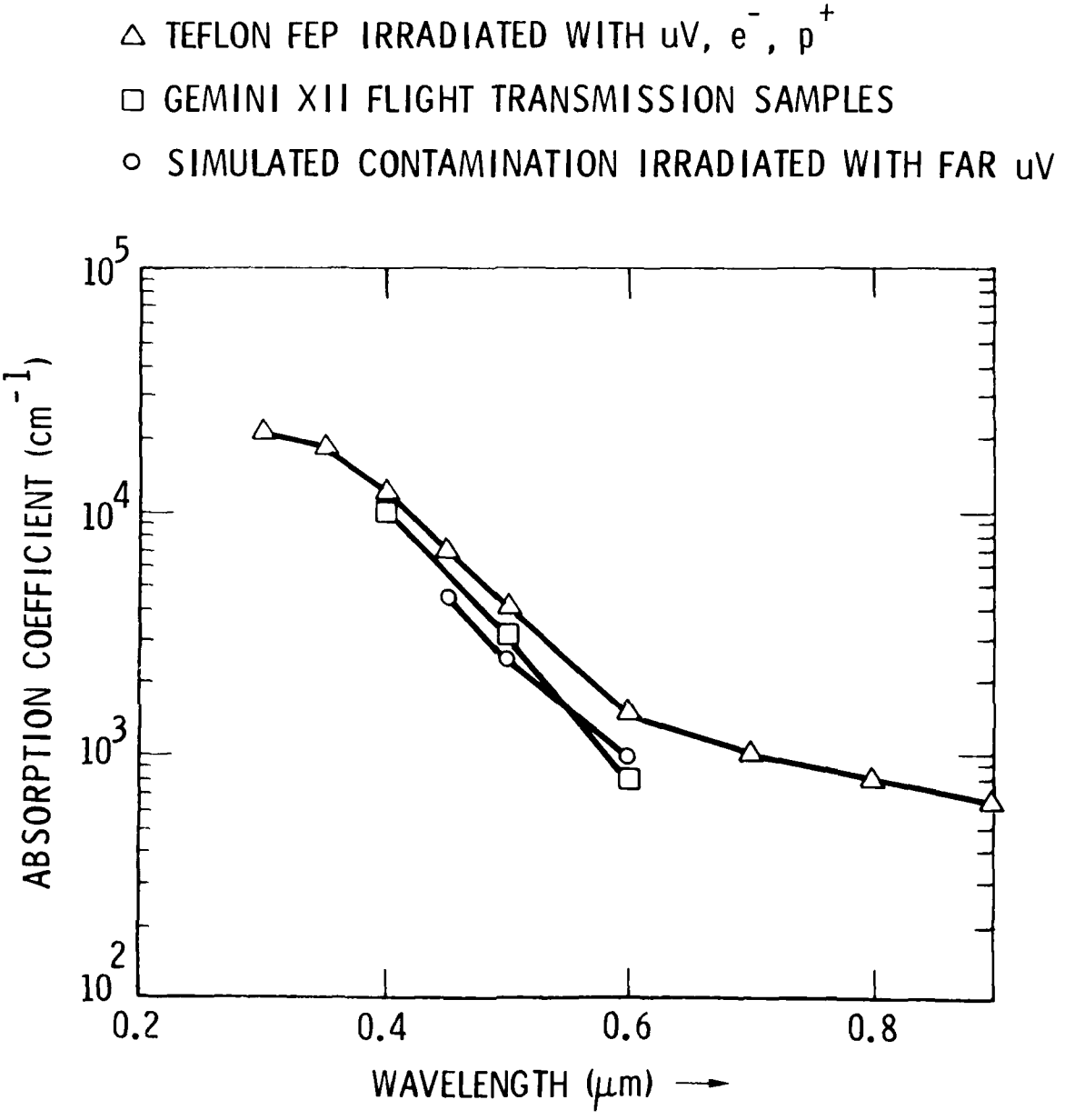

Fig. 26. Absorption Coefficient Vs. Wavelength of Irradiated Contaminants and Teflon FEP (after Champetier, Ref. 45). Curve denoted o was calculated from lab data (Ref. 46) on far-UV-irradiated simulated contamination. Curve denoted □ is data from Gemini XII flight transmission samples (Ref. 47). Curve denoted Δ was calculated from lab data (Ref. 48) on UV- and charged-particle-irradiated Teflon FEP.

SECTION IV
SUMMARY AND CONCLUSIONS

The experiment has been and continues to be a success. In this section the major findings to date are summarized and some of the opportunities to acquire further benefits from this resource are indicated.

1. MAJOR RESULTS AND THEIR IMPACTS

Degradation of Fused Quartz Mirror Radiators

Most AF satellites employ heat radiators, which are mosaics of second surface fused quartz mirrors, to reject heat from the vehicle. Invariably, these radiators degrade at a rate that is substantially greater than that of the OCLI SI-100 mirror sample on ML12-3. The very low degradation rate of the ML12 mirror is due to the relatively small amount of contamination that arrives at its outer surface and the inherent optical stability of the mirror in the space environment. Unlike the typical radiator, the ML12 mirror has a virtually clear field of view. This means contamination molecules must reach it by non-line-of-sight processes, which are less "efficient" than line-of-sight processes.

From this information it is concluded that (1) the most fruitful way to increase radiator end-of-life performance is to reduce the contamination it collects, and (2) there is much room for improvement in satellite radiator performance.

Non-line-of-Sight Contamination Transport

Since the space-stable thermal control coating samples (fused quartz mirror, polished aluminum) and the equatorial band TQCM collected contamination, it is clear that non line-of-sight transport of contamination molecules does occur. Two transport processes are believed important at high altitudes: backscatter of contaminants off molecules outgassed or vented from the vehicle and electrostatic reattraction of ionized contaminants. Therefore, spacecraft designers should be aware of non line-of-sight transport, and their designs should reflect this knowledge.

Effect of Spacecraft Charging on Contamination Rate

In the case of the ML12 experiment on P78-2, long-term average mass accumulation rates were approximately 25% greater when 0 to 500 eV ions were allowed to reach the mass detector than when they were reflected. These ions must have been electrostatically re-attracted to the vehicle when its frame was negatively charged. This implies that in spacecraft design, charge control measures should be considered for contamination sensitive surfaces.

Optical Properties of Thin Films of P78-2 Spacecraft Contamination

When the increase of fused quartz mirror solar absorptance with time is divided by the increase of mass on the nearby TQCM with time, it is found that, at least over the first 500 Å, the change in solar absorptance per unit thickness is linear with a sensitivity of approximately 1.3×10^{-5} solar absorptance units per angstrom. Here a unit density uniform film has been assumed to convert mass per unit area into thickness. This sensitivity is 1/8 the value that has often been used in the past for worst case analysis.

Role of Sunlight in Contamination Buildup

Comparison of the data from the sunlit and shadowed TQCMs reveal striking differences. Contamination adsorbs much more readily on the sunlit detector and adheres to it much more tenaciously. This implies that there are considerable advantages to shadowing contamination sensitive spacecraft surfaces from sunlight. This result also raises questions as to the applicability of the ASTM 595 materials outgassing screening test when the collecting spacecraft surface receives sunlight.

Contamination Accumulation

Contamination continues to accumulate on spacecraft surfaces for years. The e-folding time constant for mass collection on the equatorial band TQCM is about 590 days. Since vehicle surface materials probably outgas more quickly than this, it is believed that molecules released from the vehicle interior are a major fraction of those collected on this detector. This implies that space vehicle vents should be well removed from contamination sensitive spacecraft surfaces.

Thermal Control Coatings Sample Equilibrium

After three years on orbit, none of the thermal control coating samples' solar absorptance values were showing signs of approaching an equilibrium value. This fact underscores the need for long term testing of coatings which are not space-stable, whether on orbit or in space simulation facilities.

Indium Oxide Coatings Degradation

Both of the thermal control coating samples that have indium oxide based transparent conductive coatings exhibited a transient increase in solar absorptance with an approximately 2-month time constant. Those employing these coatings for control of surface charging should expect to pay a total penalty of approximately 0.04 solar absorptance units.

Contamination from Thrusters Bounded

Considerable effort was expended analyzing the flight data for evidence of contamination collection by the ML12 sensors associated with firing the solid and various liquid propellant thrusters on P78-2. No evidence was found. Therefore, the sensitivities of the instruments establish upper bounds for contamination collected at the sensor locations from these potential sources. In the case of the solid propellant thruster firing, approximately 2.4 ng/cm^2 could be detected, whereas in the cases of the liquids the detection thresholds were between 5 and 8 ng/cm^2.

2. Future Activities

The AF Space Test Program intends to operate P78-2 and collect 24 hours worth of data per day until the Satellite Control Facility (SCF) Data System Modernization (DSM) program is implemented in 1987, or until the vehicle has a sufficiently serious failure to make its continued operation impractical.

AFWAL intends to continue funding ML12 operation, data analysis, and dissemination at least through FY 85. Thus, opportunity will exist to increase the store of information produced by this experiment.

As a matter of fact, even if ML12 or P78-2 should fail immediately, there is already in hand a great deal of valuable data awaiting analysis.

In the following sections some of the topics available for future study are discussed briefly. Currently contemplated funding levels will not permit work on all of these topics.

a. Previously Acquired Data

Spacecraft Contamination

Much more work could be done with existing data to improve understanding of spacecraft contamination processes. Opportunities exist in the areas of contamination transport, contamination characteristics, comparison of contamination models with the data, and anomaly investigations.

Two processes are believed important in transporting contaminant molecules to the ML12 detectors: scattering and electrostatic reattraction. A significant amount of scattering is suspected to occur in the flow of outgassed molecules venting from the interior of the vehicles. It would be very instructive to compare the ML12 mass accumulation data with an estimate of the flux arriving at the detectors by this means. Also, data obtained in the highly elliptical transfer orbit have not been analyzed.

As regards the electrostatic reattraction mechanism, several possibilities exist for further work. Additional analyses can be done using the same (statistical) techniques as were already used with ML12-6 data (described on page 50 and following). These analyses could employ data from additional periods during the flight, and also data from ML12-7. It also may be possible to find periods of natural P78-2 charging in sunlight of sufficient duration and intensity to be directly observable in the ML12 TQCM data. However, identification of periods of charging would require use of data from other instruments (SC9, SC2, or SC10) to detect the charging, and would therefore be time consuming, and probably require extensive computer time. There were a few extended periods of artificial spacecraft charging by SC4-2 at ML12 request. It is expected that magnetic tapes of the data from these periods will become available in FY84. Finally, data during natural or artificial P78-2 charging

from the SC8 mass spectrometer in the "heavy ion" mode may contain evidence of contaminant ions, or fragments thereof, which were electrostatically reattracted.

More information could be obtained on the physical characteristics of the P78-2 contamination through more detailed study of the dependence of adsorption and desorption rates on TQCM temperature. However, a thorough study in this area would require correcting the data for the TQCM's own response to changes in temperature. Though achievable, this would be a significant task. Also, data obtained during the first few days of flight have not been analyzed in detail.

Several orgainizations have developed models for the prediction of contamination deposition on spacecraft surfaces and its optical effects. Some models are restricted to thruster effluents, whereas others are more general. If one or more of these models were used to successfully predict deposition on the ML12 detectors, confidence in the model would be increased greatly.

There have been several anomalies in the ML12 data. For instance, ML12-7 has occasionally changed mass reading nearly instantaneously, as if struck by a micrometeoroid. On another occasion ML12-7 suddenly began to accumulate mass at a rate many times greater than normal. When the ML12-7 temperature was raised a few months later, this mass desorbed. Although these events will probably never be explained with complete certainty, detailed analysis would yield probable explanations.

Thermal Control Coating Degradation

More work with the existing TCC data would also be fruitful. For instance, much more should be done to compare the ML12 data with those of other flights and of ground simulations. This would yield information on such matters as the relative importance of contamination versus coating material degradation and the relative importance of the various components of the space environment, and could help identify which aspects of a ground simulation are most important.

Other aspects of the ML12 data that could be exploited are transfer orbit data, TQCM radiator degradation data, decreasing uncertainties in the solar absorption values through specialized techniques, and study of the time dependence of sample emittance. In theory, a sample emittance value may be deduced from its rate of cool down as the vehicle enters eclipse.

Space Plasma Dynamics

One of the standard instruments used in experimental plasma physics is the retarding potential analyzer (RPA). Indeed, the SC-6 experiment on P78-2 was a pair of RPAs. Unfortunately, these instruments failed during launch and produced no flight data. However, both ML12-6 and ML12-7 contain RPAs that are working well.

Three classes of investigations could be conducted with the ML12 RPA data. These are studies of the properties of the low energy ambient plasma as a function of various vehicle and geomagnetic conditions, studies of the return flux of charged particles that were emitted by the SC4 ion and electron sources, and partial validation of the NASCAP computer code.

The population of low energy electrons in the ambient plasma is believed to change significantly during conditions that produce spacecraft charging. Most charged particle instruments, including the others on P78-2, do not work reliably below about 100 eV. The ML12 RPA has grid bias steps at 0, -1, -10, and -100 volts and could therefore be used to study electrons between 0 and 100 eV as a function of parameters of interest.

Some of the charge particles that are released by the electron and ion guns on the vehicle are returned to the vehicle by electrostatic and magnetic forces. Study of these fluxes will yield information on the forces and the utility of active spacecraft potential control with charged particle guns.

b. Future Data

Since the Space Test Program will continue to collect vehicle data until about 1987, opportunities to acquire additional information will exist in the following areas.

Long Term Effects

An emphasis of Space Division over the last decade has been to increase the operational life of space vehicles. Today the goal is often 10 years. Obviously, to design for a realistic end-of-life performance of subsystems, long term degradation rates must be known. Contamination and materials optical degradation often affect spacecraft thermal and sensor performance, and sometimes that of solar arrays as well. Continued analysis and publication of ML12 data will provide a much firmer basis upon which to extrapolate coatings performance and contamination accumulation to 10 years on orbit. Indeed, the coatings data reported herein do not indicate that equilibrium values of solar absorptance will be obtained. Of course, they must equilibrate at a value less than unity. The mass accumulation on the equatorial band TQCM does suggest that its final value will be in the range of 6 to 8 mg/cm^2, but most people would feel more comfortable with additional data.

Future Experiments

The capabilities of the instruments have not yet been fully exercised, and some past experiments will bear repetition. For instance, it is possible to command six of the first- and second-surface mirror samples to four different temperatures. This capability was provided to see if adsorbed contaminants could be desorbed by heating. Utilization of the capability has been postponed until the samples had a clearly measurable solar absorptance increase. Some of these heating experiments are planned for FY 84.

Other classes of likely future experiments are filling data voids and investigating uncertainties that become apparent during analysis of previously acquired data. This can be accomplished by actively commanding the instruments.

Finally, it is also possible that the natural environment of the spacecraft will provide conditions that are unique in degree if not kind. For example, one of the most active periods of P78-2 charging since launch occured in the Fall 1983.

Space Plasma Dynamics

As in the case of previously collected data, study of the features of the environment that produce future charging events, electric discharges, and SC4 return fluxes are likely to be of interest.

Anomaly Investigations

It is reasonable to expect that there will continue to be occasional surprises in the ML12 data. Perhaps as this data base increases, the explanations for past surprises will become more clear.

In summary, the current and future ML12 data sets are a very large supply of a usually very scarce commodity: reliable flight data concerning contamination characteristics and transport. Continued analysis of this data will likely yield additional valuable information.

REFERENCES

1. DeForest, S. E., and McIlwain, C. E., "Plasma Clouds in the Magnetosphere," J. Geophys. Res. 76, 3587 (1971).

2. DeForest, S. E., "Spacecraft Charging at Synchronous Orbit," J. Geophys. Res. 77, 651 (1972).

3. McPherson, D. A., Cauffman, D. P., and Schober, W. R., "Spacecraft Charging at High Altitudes: SCATHA Satellite Program," J. Spacecraft and Rockets 12, 621-626 (1975).

4. Rosen, A., ed., Spacecraft Charging by Magnetospheric Plasmas, Progress in Astronautics and Aeronautics 47, AIAA, MIT Press, Cambridge, Mass., and London (1976).

5. Rosen, A., "Spacecraft Charging: Environment-Induced Anomalies," J. Spacecraft and Rockets 13, 129-136 (1976).

6. Pike, C. P., and Lovell, R. R., eds., Proceedings of the Spacecraft Charging Technology Conference, AFGL-TR-77-0051, NASA TMX-73537, National Technical Information Service, Springfield, Va. (1977).

7. Spacecraft Charging Technology-1978, AFGL-TR-79-082, NASA Conference Publication 2071, Scientific and Technical Information Office, NASA, Washington, D.C. (1979).

8. Cauffman, D. P., Ionization and Attraction of Neutral Molecules to a Charged Spacecraft, TR-0074(9260-09)-1, The Aerospace Corp., El Segundo, Calif. (1973).

9. Hall, D. G., et al., Experiment to Measure Enhancement of Spacecraft Contamination by Spacecraft Charging, NASA SP-379, National Technical Information Service, Springfield, Va. (1975).

10. Lovell, R. R., et al., "Spacecraft Charging Investigation: A Joint Research and Technology Program," Spacecraft Charging by Magnetospheric Plasmas, A. Rosen, ed., Progress in Astronautics and Aeronautics 47, AIAA, MIT Press, Cambridge, Mass., and London.

11. Stevens, J. R., and Vampola, A. L., eds., Description of the Space Test Program P78-2 Spacecraft and Payloads, SAMSO-TR-78-24, National Technical Information Service, Springfield, Va. 1978.

12. Fennell, J. F., "Description of the P78-2 (SCATHA) Satellite and Experiments," The IMS Source Book, American Geophysical Union, 1982, pp. 65-81.

13. "Vacuum Stability Requirements of Polymeric Materials for Spacecraft Applications," NASA-SP-R-0022, Rev. A (9 Sept. 1974).

14. Clippinger, D., "P78-2 Parts, Materials, and Processes Selection and Control Requirements--Materials Selection List," Martin Marietta Corp., Denver, Colo., Doc. No. 85800010205, Rev. G (16 June 1978).

15. Clippinger, D., "P78-2 Product Cleanliness Levels, Clean Area Control, and Contamination Control Requirements," Martin Marietta Corp., Denver, Colo., Doc. No. 85800010505, Rev. A, Oct. 1976.

16. "Military Standard Product Cleanliness Levels and Contamination Control Program," Department of Defense, Washington, D.C., MIL-STD-1246A, 18 Aug. 1967.

17. "Federal Standard Clean Room and Work Station Requirements, Controlled Environment," General Services Administration, Washington, D.C., Fed. Std. No. 209B, Nov. 1974.

18. "Clean Area Control," Rev. G., Martin Marietta Corp., Denver, Colo., Doc. No. STP 72102, Nov. 1974.

19. "Space Test Program Flight P78-2 Space Vehicle/Launch Vehicle ICD," Martin Marietta Aerospace, Denver, Colo., CDRL A050, 8 Apr. 1977.

20. "Delta Spacecraft Design Restraints," McDonnell Douglas Corp., Huntington Beach, Calif., Doc. No. DAC 61687B, May 1976.

21. Berliner, E., "Design Considerations and Operational Performance of P78-2 (SCATHA) Program Reaction Control System," Paper No. AIAA-80-1295, AIAA/SAE/ASME 16th Joint Propulsion Conference, Hartford, Conn., 30 June 1980.

22. Carre, D. J., and Hall, D. F., "Contamination Measurements During the Operation of Hydrazine Thrusters on the P78-2 (SCATHA) Satellite," J. Spacecraft Rockets 20, 444 (1983).

23. Fote, A. A., and Hall, D. F., "Contamination Measurements During the Firing of the Solid Propellant Apogee Insertion Motor on the P78-2 (SCATHA) Spacecraft," Proceedings of the Society of Photo-Optical Instrumentation Engineers, Vol. 287, Shuttle Optical Environment, 1981.

24. Luedke, E. E., and Kelley, L. R., "Development of Flight Units for Thermal Control Coatings Experiment," AFML/MBE, Wright-Patterson Air Force Base, Ohio, AFML-TR-72-233, 1972.

25. Steen, P. G., "SCATHA Experiment Shadowing Study," Systems, Science, and Software, LaJolla, Calif. SSS-R-78-3658 (1978).

26. Pettit, R. B., "Evaluation of Portable Optical Property Measurement Equipment for Solar Selective Surfaces," Journal Engineering for Power, Vol. 100, 1978, p. 489.

27. Thekaekara, M., "The Solar Constant and the Solar Spectrum Measured from a Research Aircraft," NASA Tech. Rept. R-351.

28. Nelson, K. E., Luedke, E. E., and Bevans, J. T., "A Device for the Rapid Measurement of Total Emittance," Journal of Spacecraft and Rockets, Vol. 3, 1966, p. 758.

29. Jakob, M., Heat Transfer, Vol. 1, Wiley, N.Y., 1949, p. 52.

30. Eagles, A. E., "Fabric Coatings for Satellite Temperature Control, Vol. II: Design Handbook," Wright-Patterson Air Force Base, AFML-TR-77-65, Vol. II, AFML/MBE, 1976.

31. Hyman, N. L., "Solar Absorptance Degradation of OSR Radiators on the COMSTAR Satellites, "AIAA 16th Thermophysics Conference, AIAA-81-1185, Palo Alto, Calif., June 23-25.

32. Ahern, J. E., and Karperos, K., "Calorimetric Measurements of Thermal Control Surfaces on Operational Satellites," Paper No. AIAA-83-0075, AIAA 21st Aerospace Sciences Meeting, Reno, Nev., 10-13 Jan. 1983.

33. Bourrieau, J., and Paillous, A., "Effect of Radiations on Polymers and Thermal Control Coatings," ESA SP-145, Proceedings of an ESA Symposium on Spacecraft Materials, December 1979.

34. Prince, D. E., "ML-101 Thermal Control Coating Spacecraft Experiment," AFML-TR-75-17, AFML/MBE, Wright-Patterson AFB, Ohio, Aug. 1975.

35. Hall, D. F., "Flight Experiment to Measure Contamination Enhancement by Spacecraft Charging," Paper No. 216-15, Optics in Adverse Environments, SPIE, Vol. 216, Bellingham, Wash., 1980, pp. 131-137.

36. Fleischauer, P. D., and Tolentino, L., "The Far Ultraviolet Photolysis of Polymethyl-phenylsiloxane Films on Quartz Substrates," NASA SP-336, U.S. Government Printing Office, Washington, D.C., 1973, pp. 645-650.

37. McKeown, D., et al., Temperature Controlled Quartz Crystal Microbalance System, AFML-TR-77-83, AFML/MBE, Wright-Patterson Air Force Base, Ohio, 1977.

38. Chater, W. T., "A Digitizing Electrometer System Using an Integrating Circuit Preamplifier," Rev. Sci. Inst. 42, No. 1, pp. 129-134, Jan. 1971.

39. Warner, A. W., and Stockbridge, C. D., in Vacuum Microbalance Techniques, Vol. 2, edited by R. F. Walker, Plenum Press, New York (1972), p. 71.

40. Hall, D. F., and Fote, A. A., 1979, Preliminary flight results from P78-2 (SCATHA) spacecraft contamination experiment, Proc. of an ESA Symposium on Spacecraft Materials, ESA SP-145, 81-89.

41. Hall, D. F., and Clark, D. M., "Preliminary Results of Contamination Measurements During P78-2 (SCATHA) Charging Event," presented to 18th AIAA Aerospace Sciences Meeting, Pasadena, Calif., Jan. 16, 1980.

42. Clark, D. M., and Hall, D. F., 1980, Flight evidence of spacecraft surface contamination rate enhancement by spacecraft charging obtained with a quartz-crystal microbalance, Proc. of Third AF/NASA Spacecraft Charging Technology Conference, NASA Conference Publication 2182, 493-508.

43. Hall, D. F., "Current Flight Results from the P78-2 (SCATHA) Spacecraft Contamination and Coatings Degradation Experiment" (ESA SP-178), Proceedings of an International Symposium on Spacecraft Materials in Space Environment, Toulouse, France, 8-12 June 1982.

44. Zeiner, E. A., 1982, Private communication, Hughes Aircraft Co. Space and Communications Group, El Segundo, Calif.

45. Champetier, R., 1981, Effects of contaminants on optical characteristics of surfaces, Spacecraft Contamination from Propulsion Systems Workshop, The Aerospace Corp., El Segundo, Calif., Sept. 22, 1981.

46. Fleischauer, P. D., and Tolentino, L., 1973, The far ultraviolet photolysis of polymethylphenylsiloxane films on quartz substrates, NASA SP-336, 645-650.

47. Rantanen, R. O., Bareiss, L. A., and Ress, E. B., 1974, Determination of Space Vehicle Contamination, Proc. of Centre National D'Etudes Spatiales Symposium on Evaluation of Space Environment on Materials, held at Toulouse, France, 211-232.

48. Kurland, R. M., Properties of Metallized Flexible Materials in the Space Environment, USAF SAMSO TR 78-71 (1978).